

AD-A112 342

SRI INTERNATIONAL MENLO PARK CA  
DIP PROCESS THERMAL BARRIER COATING FOR SUPERALLOYS. (U)

F/6 11/6

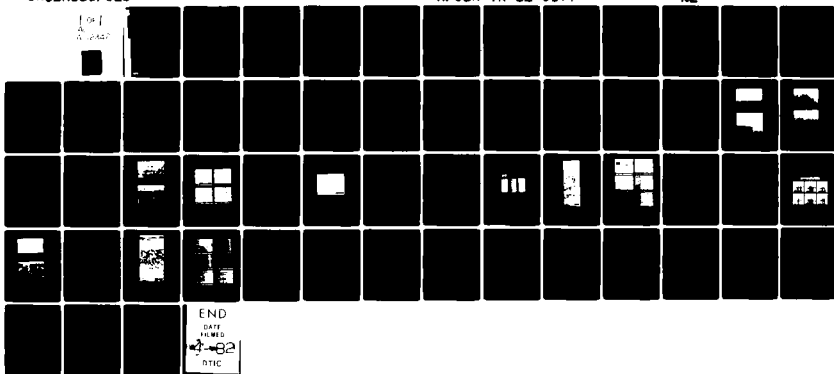
FEB 82 I M ALLAM, D J ROWCLIFFE F49630-81-K-0009

UNCLASSIFIED

AFOSR-TR-82-0177

NL

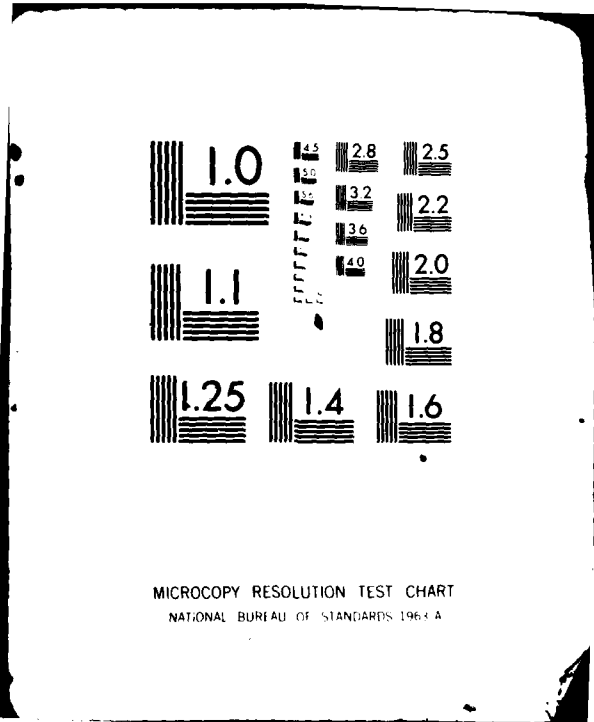
100  
A-242



END

DATE  
FILED

4-82  
RTIC



AD A 112342

AFOSR-TR- 82 - 0177

(12)

# DIP PROCESS THERMAL BARRIER COATING FOR SUPERALLOYS

February 2, 1982

Annual Report  
Covering Period December 14, 1980 to December 14, 1981

By: I. M. Allam and D. J. Rowcliffe

DATA SHEET COPY

Prepared for:

AIR FORCE OFFICE OF SCIENTIFIC RESEARCH  
Building 410  
Bolling AFB, Washington DC 20332

Attention: Captain Steven G. Wax  
Program Manager  
Electronic and Material Sciences

Contract F49630-81-K-0009

SRI Project PYU 2509



SRI International  
333 Ravenswood Avenue  
Menlo Park, California 94025  
(415) 326-6200  
TWX: 910-373-2046  
Telex: 334 486



Approved for public release;  
distribution unlimited.

Unclassified

SECURITY CLASSIFICATION OF THIS PAGE (When Data Entered)

REPORT DOCUMENTATION PAGE		READ INSTRUCTIONS BEFORE COMPLETING FORM
1. REPORT NUMBER <b>AFOSR-TR- 82 - 0177</b>	2. GOVT ACCESSION NO. <i>40-412343</i>	3. RECIPIENT'S CATALOG NUMBER
4. TITLE (and Subtitle) DIP PROCESS THERMAL BARRIER COATING FOR SUPERALLOYS	5. TYPE OF REPORT & PERIOD COVERED Annual 12-14-1980 to 12-14-1981	6. PERFORMING ORG. REPORT NUMBER PYU 2509
7. AUTHOR(s) I. M. Allam and D. J. Rowcliffe	8. CONTRACT OR GRANT NUMBER(s) F49620-81-K-0009	
9. PERFORMING ORGANIZATION NAME AND ADDRESS SRI International 333 Ravenswood Avenue Menlo Park, California 94025	10. PROGRAM ELEMENT, PROJECT, TASK AREA & WORK UNIT NUMBERS <i>611021- 2306/412</i>	
11. CONTROLLING OFFICE NAME AND ADDRESS Air Force Office of Scientific Research <i>Balloch AFB, DE 20332</i>	12. REPORT DATE February 12, 1982	13. NUMBER OF PAGES 55
14. MONITORING AGENCY NAME & ADDRESS(if different from Controlling Office)	15. SECURITY CLASS. (of this report) Unclassified	15a. DECLASSIFICATION/DOWNGRADING SCHEDULE na
16. DISTRIBUTION STATEMENT (of this Report)  Approved for public release; distribution unlimited.	17. DISTRIBUTION STATEMENT (of the abstract entered in Block 20, if different from Report)  <i>1332</i>	
18. SUPPLEMENTARY NOTES		
19. KEY WORDS (Continue on reverse side if necessary and identify by block number) Superalloys, thermal barrier coatings, rare earth, hot dipping.		
20. ABSTRACT (Continue on reverse side if necessary and identify by block number) A new, cerium oxide-base thermal barrier coating for superalloys has been investigated. Cerium oxide is promising as a thermal barrier because of its low thermal conductivity and its relatively high coefficient of thermal expansion, suggesting good compatibility with superalloys. The coating is applied by hot-dipping superalloy substrates into a molten bath of low-melting cerium-nickel alloy. Annealing and selective oxidation of cerium at low oxygen activities produce a duplex coating of a continuous outer layer of cerium oxide ( $CeO_2$ ) and an inner composite cerium oxide/substrate layer.		

Unclassified

SECURITY CLASSIFICATION OF THIS PAGE(When Data Entered)

The effect of coating composition and processing variables on the micro-structure and integrity of the coating on nickel- and cobalt-base alloys was studied in detail. The best, thin, crack-free coatings were produced on MAR-M509 with a coating alloy of Ce-30% Ni. Isothermal and cyclic oxidation tests showed that coating spallation could occur and was associated with the oxidation of nickel and cobalt incorporated in the coating. A model for the formation of the CeO<sub>2</sub> barrier and the subscale region is proposed that accounts for the presence of unwanted nickel and cobalt; methods for avoiding their presence are proposed.

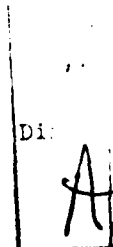
Unclassified

SECURITY CLASSIFICATION OF THIS PAGE(When Data Entered)

## PROFESSIONAL CONTRIBUTION

The Principal Investigator on this program is Dr. Ibrahim M. Allam, Materials Scientist and the Project Supervisor is Dr. David J. Rowcliffe, Program Manager, Ceramics. Dr. Kai-Hung Lau, Materials Chemist performed the thermogravimetric oxidation study, Mr. Jan C. Terry, Supervisor of the SEM Facility was responsible for the SEM analysis, and Mr. Eldon P. Farley, Research Ceramist, carried out the x-ray diffraction studies.

✓



AIR FORCE  
NOTICE  
This is to approuve  
Distribution  
MATTHEW L. ALLAM  
Chief, Technical Information Division  
AF SCIENTIFIC RESEARCH (AFSC)  
TO DDCI  
that has been made available  
by AFSC to DDCI  
is unlimited.  
DDC  
AFSC

## CONTENTS

	Page
<b>PROFESSIONAL CONTRIBUTION.....</b>	<b>iii</b>
<b>FIGURES .....</b>	<b>v</b>
<b>TABLES .....</b>	<b>vii</b>
<b>I INTRODUCTION.....</b>	<b>1</b>
A. Background.....	1
B. Objectives.....	2
C. Summary of Work: Year 1 .....	4
D. Summary of Work: Year 2.....	5
<b>II EXPERIMENTAL.....</b>	<b>7</b>
A. Materials.....	7
B. Coating Technique.....	7
1. Hot Dipping.....	7
2. Annealing.....	12
3. Internal Oxidation.....	12
4. Recrystallization Annealing.....	13
C. Evaluation Techniques.....	14
<b>III RESULTS.....</b>	<b>15</b>
A. Hot Dipping.....	15
B. Annealing.....	15
C. Internal Oxidation.....	23
1. MAR-M509.....	23
2. CoCrAlHf.....	31
3. Nickel-Base Alloys.....	31
D. Recrystallization Annealing.....	34
E. Evaluation.....	38
<b>IV GENERAL DISCUSSION.....</b>	<b>42</b>
<b>V FUTURE WORK.....</b>	<b>46</b>
<b>VI PUBLICATIONS, PRESENTATIONS, AND PATENTS.....</b>	<b>47</b>
<b>REFERENCES.....</b>	<b>48</b>

## FIGURES

	Page
Figure 1 Phase Diagram of Ce-Ni.....	9
Figure 2 Phase Diagram of Ce-Co.....	10
Figure 3 Schematic Diagram of Hot-Dipping Apparatus.....	11
Figure 4 Cross Sections of Alloy Substrates After Hot Dipping in Ce-30% Ni.....	17
Figure 5 Cross Sections After Hot-Dipping in Ce-30% Ni.....	18
Figure 6 Cross Sections of Nickel-Base Substrates After Hot-Dipping in Ce-30% Ni at 850°C Followed by Annealing in Pure Argon at 900°C for 4 Hours.....	21
Figure 7 Concentration Profiles Showing the Distribution of Ce, Co, Cr, and Ni Cross Coated Alloy Substrate MAR-M509 Following Hot-Dipping in Ce-30% Ni at 720°C and Annealing at 900C for 15 Hours.....	22
Figure 8 Cross Section of Alloy Substrate Co-25% Cr-6% Al-0.5 Hf After Hot-Dipping and Annealing at 900°C for 4 hours.....	24
Figure 9 Surface Morphologies of the Alloy Mar-M509.....	27
Figure 10 Cross Section of Coated MAR-M509.....	28
Figure 11 Concentration Profiles of Ce, Ni, Co, Cr, and W Across Coated MAR-M509 Specimen Shown in Figure 10.....	29
Figure 12 Microstructure and Analysis of Coated Co-25% Cr-6% Al-0.5% Hf.....	32
Figure 13 Cross Sections of Alloy Substrates.....	33
Figure 14 Cross Section of Coated MAR-M509.....	35
Figure 15 Concentration Profiles of Ce, Ni, Co,Cr, La, and W Across Coated MAR-M509 Specimen (Shown in Figure 14 ) After Receiving Final Recrystallization Annealing.....	36

<b>Figure 16</b> Isothermal Weight Gain Versus Time Plot for Uncoated (Curve 1) and Coated (Curve 2) MAR-M509; Curve 3 and 4 Correspond to Samples that Received Final Recrystallization Annealing.....	39
<b>Figure 17</b> Results of Preliminary Evaluation of Spallation Resistance of Coated and Uncoated MAR-M509 Under Thermal Cycling Conditions.....	41

**TABLES**

	<b>Page</b>
<b>Table 1 Properties of Ceria (<math>CeO_2</math>) and Stabilized Zirconia (<math>ZrO_2</math>).....</b>	<b>3</b>
<b>Table 2 Alloy Substrate Compositions.....</b>	<b>8</b>
<b>Table 3 Results of Step 1, Hot Dipping.....</b>	<b>16</b>
<b>Table 4 Conditions and Results of Annealing.....</b>	<b>19</b>
<b>Table 5 Conditions and Results of Internal Oxidation.....</b>	<b>25</b>

## I INTRODUCTION

### A. Background

The ever increasing demand for higher turbine inlet temperature in gas turbines has created an extensive interest in using ceramic materials to protect airfoil surfaces. During the past decade, a concentrated effort was devoted to developing ceramic thermal barrier coatings to improve turbine durability by reducing metal temperatures, and to improve thermal efficiency by allowing operation at higher firing temperatures and with less cooling air.

Stabilized zirconia ( $ZrO_2-Y_2O_3/MgO/CaO$ ) has evolved as a prime candidate for such use, principally because its thermal conductivity is low,<sup>1-3</sup> and its coefficient of thermal expansion is relatively close to that of superalloys.<sup>1,2,4,5</sup> Various techniques have been used to apply ceramic coatings including plasma spraying,<sup>4</sup> sputtering,<sup>6</sup> and electron beam physical vapor deposition.<sup>7</sup> Each of these techniques, however, has several limitations.

Plasma spraying can lead to variable coating thickness, bare spots, pinholes, and microcracks, all of which contribute to catastrophic failure. Sputtering is expensive and limited to line of sight. Electron beam physical vapor deposition is expensive, limited to line of sight, and tends to vary coating composition because of the different vapor pressures of the constituent elements. Unlike metallic coatings, ceramic coatings are not self-healing, and once cracked or spalled, cannot be replenished from elements in the substrate. Thus it is very important to have a reliable method to produce a high quality ceramic coating for proper substrate protection.

In response to this need for improved coatings, SRI International developed a new approach, radically different from contemporary processing, that provides a cerium oxide-base thermal barrier coating for superalloys. The idea was stimulated by an earlier program at SRI<sup>8,9</sup> that studied the rapid selective internal oxidation of rare-earth cobalt alloys at relatively modest temperatures. Cerium oxide ( $CeO_2$ ) was chosen because, in

addition to its high thermodynamic stability, it has a relatively high coefficient of thermal expansion and a very low thermal conductivity compared with most other oxides.

Table 1 shows a comparison of some of the properties of ceria ( $\text{CeO}_2$ ) and stabilized zirconia ( $\text{ZrO}_2$ ).

From the coating standpoint, the most important properties of a thermal barrier oxide are:

- Coefficient of thermal expansion, which determines the coating/substrate adhesion.
- Thermal conductivity, which determines the insulating performance of the coating.
- Free energy of formation, which determines the stability of the coating at temperature.

The properties shown in Table 1 indicate that ceria has a closer coefficient of thermal expansion to that of superalloys ( $\approx 18 \times 10^{-6}/^{\circ}\text{C}$ )<sup>4</sup>. A second advantage is that the thermal conductivity of ceria is about 50% less than that of zirconia.

The new approach was developed during the first year of the program<sup>15</sup> and is based on coating superalloys with low-melting alloys, rich in cerium, and then heat-treating to develop a graded oxide layer as a thermal barrier. The current report describes progress during the second year and emphasizes the optimization of the coating procedure and preliminary evaluation of coated superalloys.

#### B. Objectives

The overall objective of this program is to develop a duplex cerium oxide-based thermal barrier coating for superalloys by a hot-dip coating process. The coating must be uniform, crack free, and adherent to underlying substrates for improved protection.

The first year objectives were to:

- (1) Determine whether the dip coating process can be applied successfully to produce reasonably uniform and adherent coatings.

Table 1  
PROPERTIES OF CERIA ( $\text{CeO}_2$ ) AND STABILIZED ZIRCONIA ( $\text{ZrO}_2$ )

Property	Stabilized Zirconia	Reference	Ceria	Reference
Crystal structure	Cubic	10	Cubic	10,11
Density (g/cc)	6.27	10	7.3	10
Melting Point ( $^{\circ}\text{C}$ )	$2770 \pm 80$ 2680	10 12	2341	1
$\Delta G_f^0$ at $1100^{\circ}\text{C}$ (Kcal/mole)	-199.7	12	-194.3	12
Dissociation pressure at $1100^{\circ}\text{C}$ (atm)	$1.64 \times 10^{-32}$	12	$5.54 \times 10^{-31}$	12
Diffusion coefficient of oxygen at $1100^{\circ}\text{C}$ ( $\text{cm}^2/\text{sec}$ )	$9.99 \times 10^{-8}$	13	$5 \times 10^{-8}$	13
Coefficient of thermal expansion ( $^{\circ}\text{C}$ )	$10 \times 10^{-6}$ (at $1000^{\circ}\text{C}$ ) $12 \times 10^{-6}$ $8 \times 10^{-6}$ $15.17 \times 10^{-6}$ (at $1100^{\circ}\text{C}$ )	4 5 2 1	$12.3 \times 10^{-6}$ ( $20-1020^{\circ}\text{C}$ ) $17.14 \times 10^{-6}$ (at $1100^{\circ}\text{C}$ )	14 1
Thermal conductivity cal/cm sec $^{\circ}\text{C}$	$4.75 \times 10^{-3}$ (at $1100^{\circ}\text{C}$ ) $5.5 \times 10^{-3}$ (at $1000^{\circ}\text{C}$ )	1 2,3	$2.07 \times 10^{-3}$ (at $1100^{\circ}\text{C}$ ) 86-92% dense	1

- 
- (2) To characterize the coating chemistry, microstructure and uniformity.

The second year objectives are to:

- (1) Optimize processing conditions and properties of the dip coating on IN738.
- (2) Evaluate thermal oxidation resistance of the optimized coating under static and thermal cycling conditions and determine whether hot strength is degraded.
- (3) Using the optimized dip coating system for IN738 to develop to a promising stage dip coatings for other superalloys, with primary emphasis on nickel-base alloys.

The third year objectives are to:

- (1) Modify the coating melt composition in order to obtain an outer cerium oxide continuous layer which contains no metallic constituents (mainly nickel and cobalt).
- (2) Determine the mechanism of internal oxidation during Step 3 of the dip coating process.
- (3) Study the resistance of the coating to hot corrosion by molten sulfate deposits.
- (4) Evaluate the hot strength of dip-coated alloys.

C. Summary of Work: Year 1

The first year of the current project established a four step process for the application of the new coating as follows:

- (1) The cerium-containing alloys are fused onto superalloys by dipping the superalloy into the coating melt.
- (2) The dipped samples are then annealed in pure argon to develop a metallurgical bond between the cerium-rich surface layer and the substrate.
- (3) Cerium is then selectively oxidized at low oxygen activity producing a cerium oxide-rich outer scale, and an inner subscale containing dispersed cerium oxide in an alloy matrix of the other elements: Co, Ni, and Cr.
- (4) Finally, the coated samples are annealed at high temperature to convert the submicron internal oxide particles into larger particles, which offers further protection by slowing the inward diffusion of oxygen into the substrate (blocking effect).

The most significant results of the first year's work include:

- (1) Step 1 (hot-dipping) and Step 3 (internal oxidation) are the most critical steps in determining the coating quality. Proper hot-dipping is obtained on nickel-base and cobalt-base alloy substrates by using relatively low melting Ce-Co coating alloys. These melts provide the best wetting, the best adhesion, and a uniform  $\text{CeO}_2$  coating layer.
- (2) Internal oxidation in a low-oxygen-activity atmosphere provides an external Ce-rich layer and a subscale composite layer of  $\text{CeO}_2$  in the residual substrate.
- (3) The coating microstructure and composition are critically dependent on the substrate composition. Preliminary results showed that the coatings on the cobalt-base alloy MAR-M509 are thinner than those on the nickel-base alloy IN-738.
- (4) Complete conversion of metallic cerium into cerium oxide was not achieved during the first year program because of the low internal oxidation temperature and the relatively short internal oxidation treatment.

The major limitations for the development of this coating were:

- (1) The use of coating melts with a high cerium content, although beneficial for proper substrate surface wetting and coverage, limits the internal oxidation temperature (Step 3) to below 450°C. At these temperatures, the  $\text{CeO}_2$  growth rate is fairly slow, and this leads to an incomplete conversion of metallic cerium to  $\text{CeO}_2$  in the surface zone.
- (2) Hot-dipping the nickel-base alloy IN738 into Ce-Co melts produces a thick interaction zone at the substrate surface, within which oxidation will occur. This reduces the remaining cross section of the substrate and degrades its load-bearing capacity.
- (3) The outer  $\text{CeO}_2$  scale formed on the nickel-base substrate was fairly incoherent and contained cracks.

#### D. Summary of Work: Year 2

To improve the coating quality, we directed a second year effort to study the proper combinations of coating and substrate alloy compositions. It was also necessary to optimize the processing conditions for the four-step coating process to produce thin, and crack-free duplex coatings. The second year effort also included a preliminary evaluation of

the oxidation behavior of optimized coatings under isothermal and thermal cyclic conditions.

During the past year, optimization of the processing conditions and evaluation of the dip-process thermal-barrier coating was conducted to produce a duplex cerium oxide ( $CeO_2$ ) coating on Ni- and Co-base superalloy substrates. The most significant results are:

- (1) Of the five compositions of the low-melting coating alloys, Ce-30% Ni performs the best.
- (2) The integrity of the duplex coating on cobalt-base alloy substrate (MAR-M509 and Co-25Cr-6Al-0.5Hf) is superior to that on nickel-base alloys (IN738 and Ni-25Cr-8Al-1Y). Coatings on MAR-M509 in particular were thin, adherent, crack free, and easily reproducible.
- (3) Hot-dipping, annealing and internal oxidation treatment of MAR-M509 produced a duplex oxide layer that is very promising as a thermal barrier. The outer scale is a continuous protective  $CeO_2$  layer and the inner layer is a subscale of  $CeO_2$  matrix and unoxidized alloy islands. The microstructure of the duplex scale changes gradually toward the substrate into a fibrous  $CeO_2$  network embedded in a matrix of the substrate alloy.
- (4) The outer scale and the subscale contain high levels of metallic nickel and cobalt incorporated during the rapid growth of  $CeO_2$ . The presence of both metals harms the coating oxidation resistance and its adherence to the substrate.
- (5) The final step, recrystallization annealing, reduces the  $CeO_2$  to the unstable  $Ce_2O_3$  and allows solid state interaction between cerium oxides and other substrate constituents that lead to the formation of complex mixed oxides; i.e.,  $0.5(La_2O_3-Cr_2O_3)$ ,  $0.5(Ce_2O_3-La_2O_3-Cr_2O_3)$ ,  $La_6WO_{12}$ , and  $(La_6, Ce_6)WO_{12}$ . Tungsten oxides in particular are volatile at higher temperatures and their presence is considered deleterious to the coating. Recrystallization annealing has thus been eliminated from the coating process.
- (6) A model was proposed that describes the mechanism of oxidation during the formation of the duplex coating and accounts for the incorporation of nickel and cobalt in the barrier structure. Based on this model, approaches were devised that should eliminate the incorporation of unwanted metals and improve the performance of the coating.

## II EXPERIMENTAL

### Materials

Table 2 shows the composition of alloy substrates studied during this program. The chemical analyses of the alloys MAR-M509 and IN-738 were provided by the supplier.

Five coating alloys have been investigated:

- (1) Ce-18% Co
- (2) Ce-18% Ni
- (3) Ce-30% Ni
- (4) Ce-25% Co
- (5) Ce-15% Co-9% Ni

The first two alloys had the lowest melting temperatures in the systems Ce-Co and Ce-Ni, Figs. 1 and 2. These compositions were originally chosen to allow hot-dipping of the substrates at temperatures as low as possible to minimize the interaction between the molten alloy and the substrate. However, these compositions are very rich in cerium which leads to excessive interaction between the substrate and the coating melt during hot-dipping. Also, the use of very low melting point coatings imposes an upper limit for the subsequent internal oxidation temperature, rendering it too low for proper internal oxidation in a practically short time. Alloys 3, 4, and 5 were chosen as a compromise between the requirement of lowering the cerium content for proper coating and of obtaining a moderate melting temperature.

### B. Coating Technique

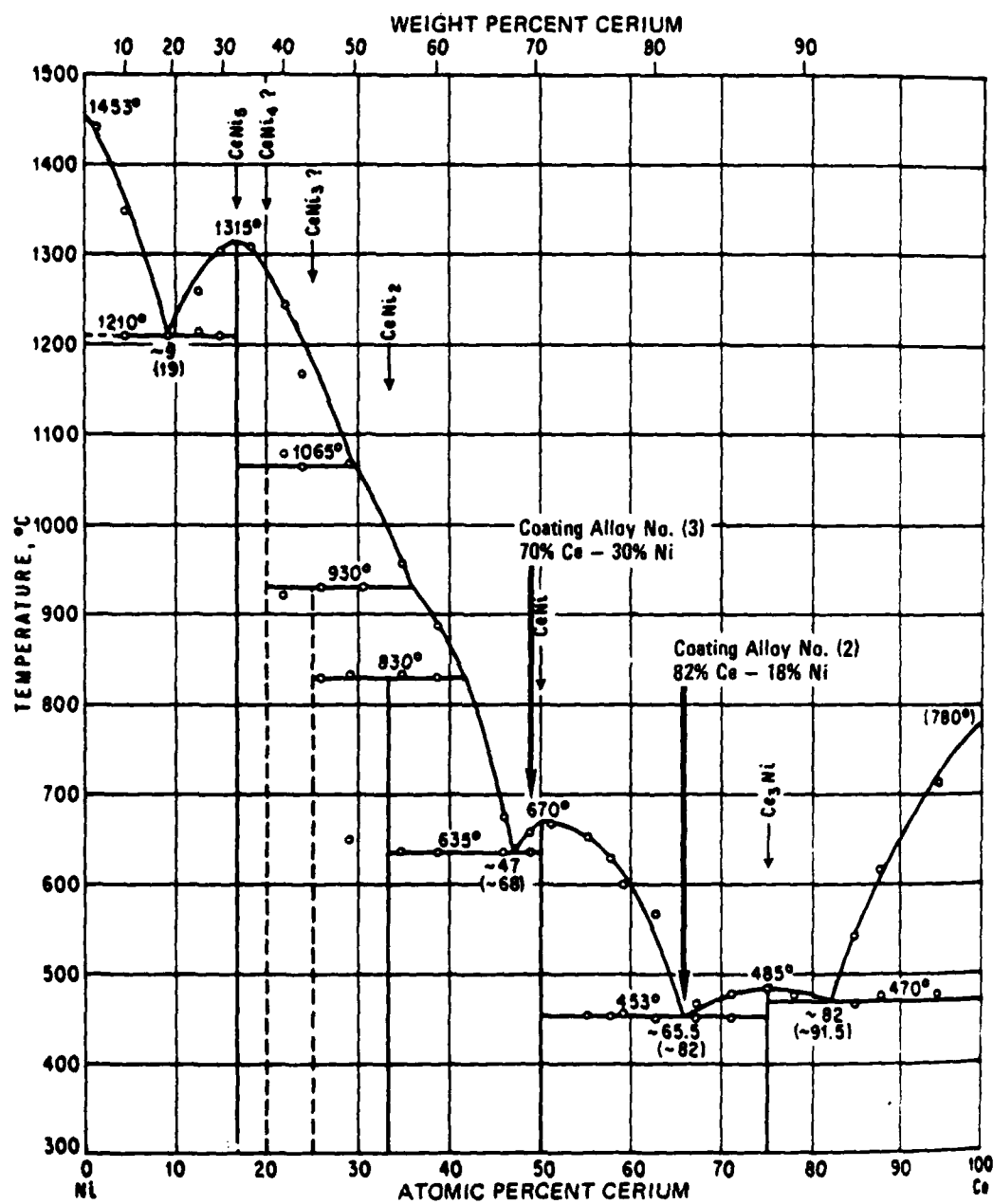
#### 1. Hot Dipping

Figure 3 shows the hot-dipping apparatus. It consists of a closed end alumina reaction chamber in a vertical resistance furnace. The coating alloy is placed in a molybdenum crucible at the bottom of the reaction

Table 2  
ALLOY SUBSTRATE COMPOSITIONS

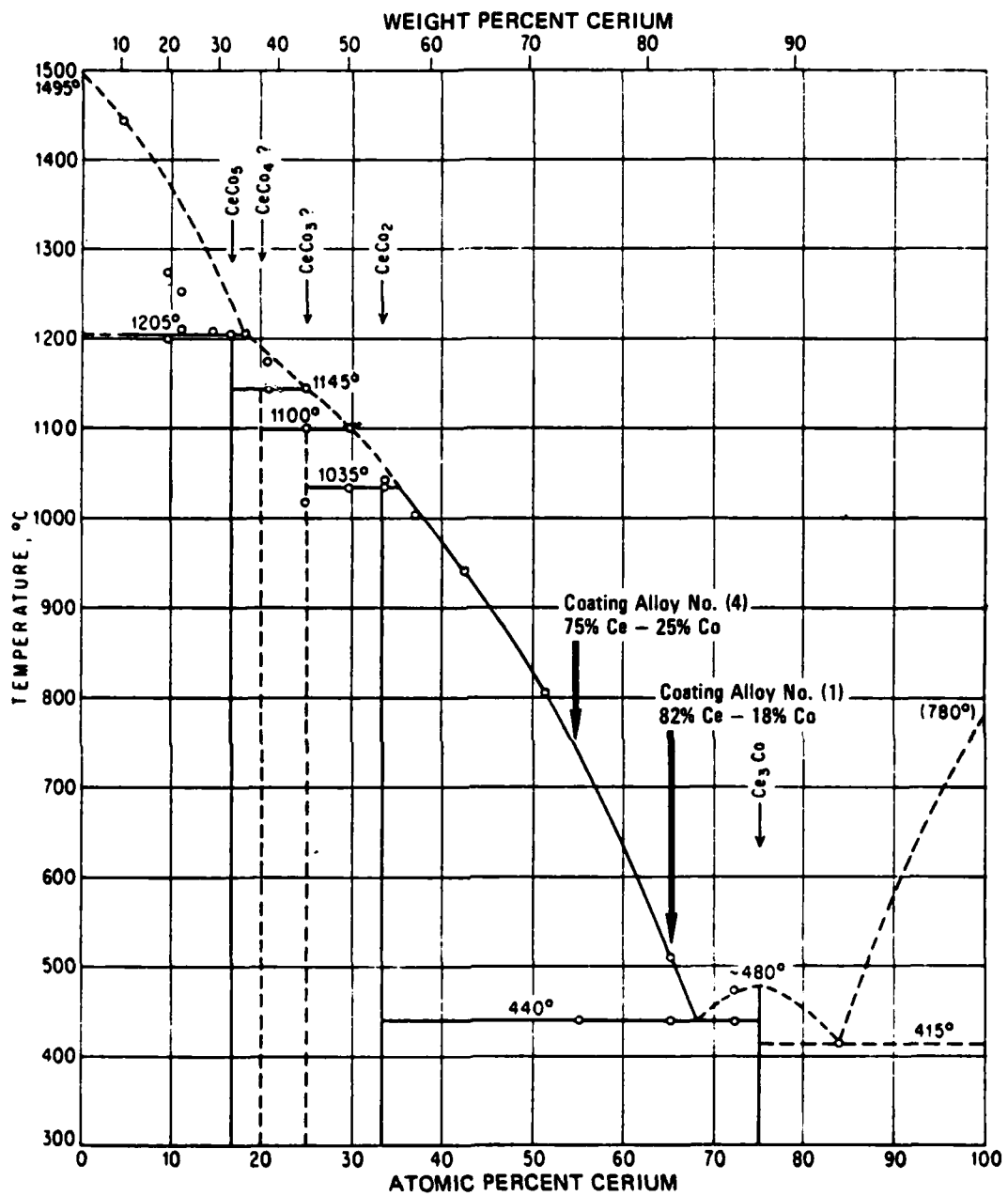
Elements	MAR M509* (wt%)	IN-738* (wt%)	NiCrAlY (wt% nominal)	CoCrAlHf (wt% nominal)
Ni	10.30	Bal	Bal	-
Co	Bal	8.37	-	Bal
Cr	23.27	16.10	25	25
Al	-	3.68	8	6
Ti	0.19	3.42	-	-
W	7.25	2.68	-	-
Ta	3.18	1.84	-	-
Fe	0.63	0.24	-	-
Mo	-	1.83	-	-
Si	0.24	0.07	-	-
Cb	-	0.81	-	-
Mn	0.01	0.007	-	-
B	0.008	0.009	-	-
Cu	0.05	-	-	-
C	0.59	0.155	-	-
S	0.004	0.003	-	-
Zr	0.43	0.08	-	-
Pb	-	1.0 ppm	-	-
Bi	-	< 0.3 ppm	-	-
Se	-	< 0.5 ppm	-	-
Te	-	< 0.5 ppm	-	-
Tl	-	< 0.5 ppm	-	-
Ag	-	< 0.5 ppm	-	-
Hf	-	< 0.5 ppm	-	0.50
Y	-	-	1	-

\*Jetshapes, Inc., Rockleigh Industrial Park, Rockleigh, NJ 07647



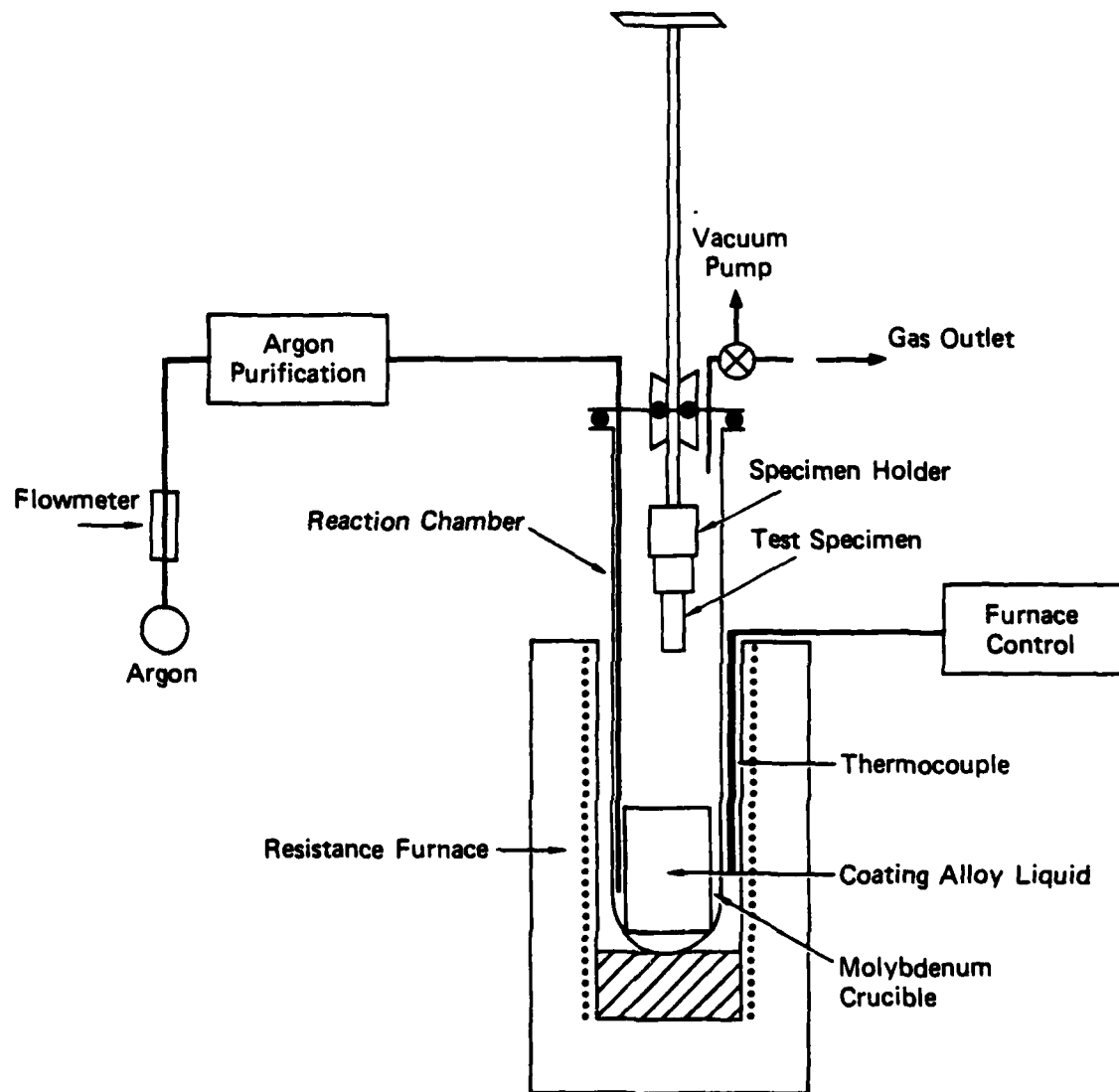
SA-8858-11A

FIGURE 1 PHASE DIAGRAM OF Ce-Ni<sup>(16)</sup>



SA-8658-10A

FIGURE 2 PHASE DIAGRAM OF Ce-Co<sup>(16)</sup>



SA-8658-1

FIGURE 3 SCHEMATIC DIAGRAM OF HOT-DIPPING APPARATUS

chamber, and the crucible temperature is monitored by a Pt/Pt-10% Rh thermocouple. Superalloy test specimens are attached to a vertical stainless steel push-rod passing through a Cajon ultra-torr fitting. Before heating, the reaction chamber is evacuated ( $10^{-5}$  atm) and then flushed with oxygen-free argon. This process is repeated several times to ensure the elimination of oxygen before melting the coating alloy. The furnace is then heated under flowing argon (10 cc/min) to the required dip-temperature. Test specimens are lowered slowly into the molten alloy and submerged, typically for 1 minute, then withdrawn.

## 2. Annealing

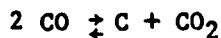
The second step of the coating process consists of annealing the dipped samples, by holding them above the melt in the dipping furnace. The annealing treatment improves the bond between the coating and substrate and reduces the cerium content, particularly within the inner portion of the coating, by diffusing cerium into the substrate so that subsequent internal oxidation of cerium leads to the formation of dispersed particles of cerium oxide-metal composite. The outer portion of the coating would remain relatively rich in cerium and, upon internal oxidation, an external continuous cerium oxide layer will develop. The reduction in the cerium content causes the surface layer to be more refractory (have a higher m.p.) than the original coating alloy.

## 3. Internal Oxidation

It was necessary to internally oxidize the coated substrates at temperatures low enough to prevent melting of the coating alloy surface layer, to prevent melting. The coated samples were internally oxidized by heating them in a gas mixture of 1% CO-99% CO<sub>2</sub>. At 600°C, the temperature at which most coated alloys received the initial internal oxidation treatment, this gas mixture provided an equilibrium oxygen partial pressure<sup>17</sup> of  $\approx 2 \times 10^{-21}$  atm. The dissociation pressures of NiO and CoO at the same temperature were  $\approx 7.2 \times 10^{-20}$  atm and  $\approx 2.5 \times 10^{-21}$  atm, respectively. Hence, little or no oxidation of Ni or Co in the coating layer or within the interaction zone was expected.

Test samples were oxidized at 600°C in CO/CO<sub>2</sub> for periods up to 70 hours to oxidize cerium selectively into a thin external layer of oxide and a composite subscale layer that contains cerium oxide particles and the unoxidized alloy. This treatment, however, appeared insufficient to completely oxidize metallic cerium in a relatively short time. Thus, further oxidation at 800°C was required to ensure complete conversion of metallic cerium into cerium oxide. The duration of this second oxidation stage depends on the thickness of the Ce-rich layer at the specimen surface. No melting of this Ce-rich layer was expected due to the low cerium gradient produced during the annealing step and due to the partial removal of cerium during the oxidation at 600°C which causes the remaining alloy to be more refractory.

To avoid any possible oxidation of cobalt or nickel, it would be preferable to oxidize the coated samples at P<sub>O<sub>2</sub></sub> lower than 2 × 10<sup>-21</sup> atm (equilibrium P<sub>O<sub>2</sub></sub> for CO/CO<sub>2</sub> = 1/99 at 600°C), which could be accomplished by increasing the CO/CO<sub>2</sub> ratio. However, an increase in this ratio results in carbon precipitation according to the Boudouard reaction



The oxygen partial pressure maintained during the first stage of internal oxidation (P<sub>O<sub>2</sub></sub> ≈ 2 × 10<sup>-21</sup> atm, CO/CO<sub>2</sub> mixture at 600°C), or that during the second stage of internal oxidation (P<sub>O<sub>2</sub></sub> ≈ 4 × 10<sup>-15</sup> atm, CO/CO<sub>2</sub> mixture at 800°C) was high enough to selectively oxidize cerium to form an external scale or an internal subscale depending on the cerium concentration at the alloy surface. Other elements, active towards oxygen, will not be oxidized, or their oxides, if formed, will be reduced by cerium.

#### 4. Recrystallization Annealing

An oxide recrystallization treatment, Step 4, was explored to convert the submicron internal oxide particles into larger, discontinuous oxide particles. The formation of a layer containing large internal oxide particles within the inner portion of the subscale may produce the "blocking effect," i.e., reduce the inward oxygen flux towards the

unoxidized substrate, which can further improve the oxidation resistance of the substrate.

This treatment involved annealing oxidized coated samples at temperatures higher than the internal oxidation temperature, typically 900 to 1000°C for up to 15 h in pure argon. At these temperatures, a dissolution-precipitation process, similar to Ostwald-ripening, can occur, where some large particles grow at the expense of many small particles.

#### C. Evaluation Techniques

The coating microstructures were metallographically examined following each of the four coating process steps. Elemental analysis of the coating constituents and their concentration profiles were conducted using SEM on sample surfaces and on cross sections. Identification of compounds within the coating layers on selected substrates was performed using x-ray diffraction analysis along planes parallel to the coating surface at various depths within the coating layers.

The oxidation behavior of coated and uncoated samples was investigated at 930°C and 150-torr oxygen pressure under isothermal oxidation conditions. Oxidation experiments on coated coupons were conducted with a continuous-recording Cahn microbalance system to measure the weight change as a function of time for various coating compositions.

Coated coupons were weighed and measured to examine the coating adhesion to underlying substrates, then placed in alumina crucibles and thermally cycled in a box furnace. Typical cycling conditions were exposure for 1 h at 1000°C in air, followed by cooling in air for about 20 min. The coupons were then brushed lightly to remove attached spalled particles and reweighed.

### III RESULTS

#### A. Hot Dipping

Table 3 shows the results of hot-dipping the four alloy substrates in different melt compositions. It is important to reduce the thickness of both the outer coating layer and the interaction zone to minimize their effects on the remaining effective cross section of the substrate alloy. Interdiffusion between both layers and the substrate during the second step (annealing) will eliminate the boundary between the two layers and cause further thickening of the total affected zone.

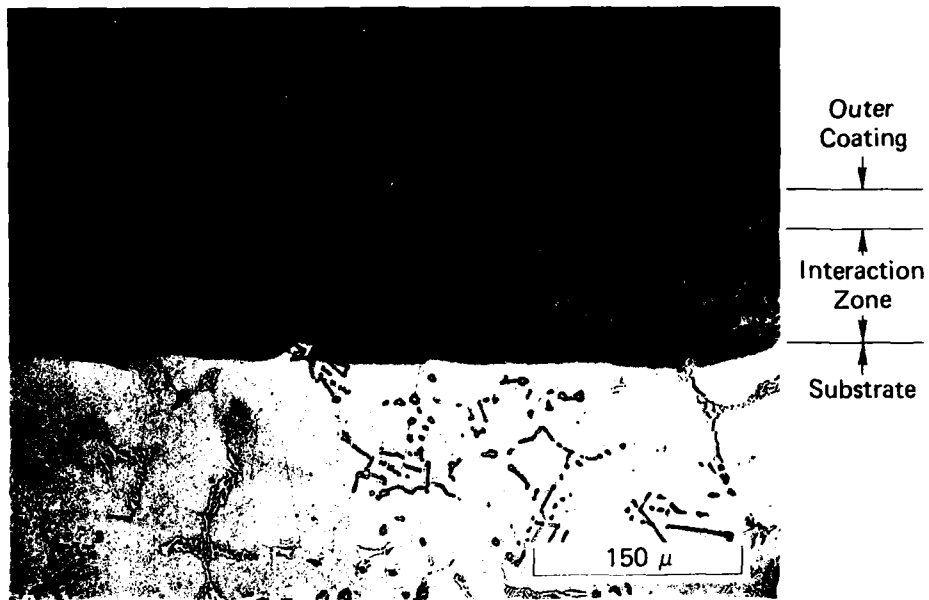
The hot-dipping results indicate that, regardless of the substrate alloy composition, the average thickness of the interaction zone can be reduced by dipping the substrates in the coating alloy Ce-30% Ni. However, the thickness of the interaction zone is also dependent on the composition of the substrate alloy, assuming a fixed dip temperature and duration. The cobalt-base alloys (MAR M509 and CoCrAlHf, Figure 4), show lower interaction zone thicknesses than the Ni-base alloys (IN738 and NiCrAlY, Figure 5), indicating that cerium atoms diffuse slower in cobalt-base alloys than in Ni-base alloys. No independent measurement for the diffusion of cerium in these alloys has been undertaken and no data were available. The best dipped layers were produced by coating alloy Ce-30% Ni on the substrate MAR-M509 at 800 to 850°C, as indicated in Table 3.

#### B. Annealing

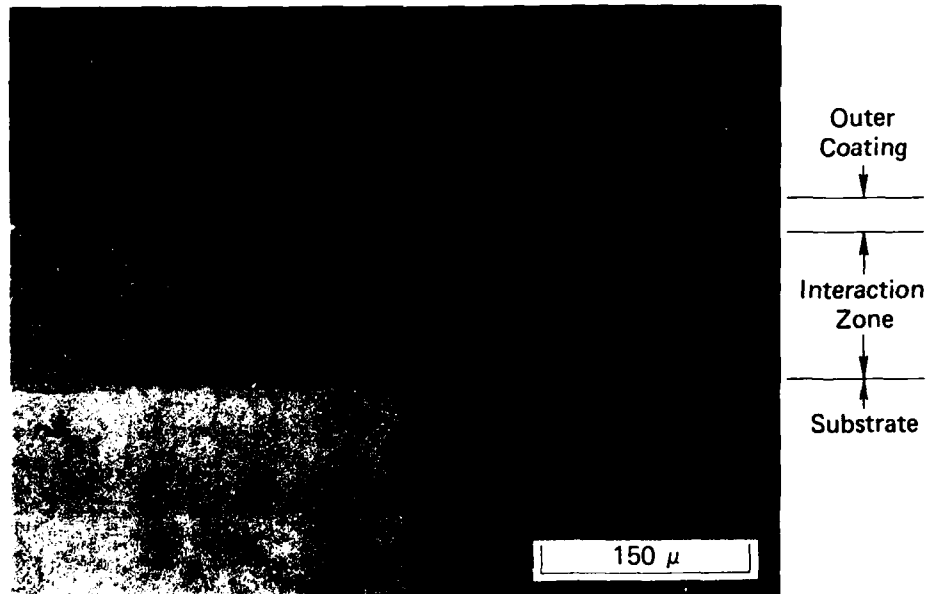
Table 4 shows the conditions and results of the annealing treatments on all four alloy substrates dipped in the coating alloy Ce-30% Ni. Substrates coated by hot-dipping into alloys 1, 2, 4, and 5 were also annealed. Annealing these coatings extensively thickened the diffusion zones and generated large pores and cracks, which led to extensive spallation.

**Table 3**  
**RESULTS OF STEP 1, HOT DIPPING**

Substrate	Sample Number	Coating Composition (wt%)	Dip Temperature for 1 min (°C)	Thickness of Outer Coating (μm)	Thickness of Interaction Zone (μm)	Remarks
IN738		Ce-18% Ni Ce-18% Co	650 650	25-35 12-62	170-215 170-214	Uneven outer coating. Interaction zone is partly adherent. Both outer coating and interaction zones are not uniform and spalled in several areas.
	(9)	Ce-30% Ni	850	25-45	= 180	Outer coating is adherent but not uniform. Interaction zone is adherent, and fairly uniform, but contains few cracks.
	(31)	Ce-30% Ni Ce-30% Ni	800 720	20 22	= 275 70-100	Both layers are uniform and adherent.
	(36)	Ce-25% Co	800	20-40	400-450	Both layers are uniform and adherent. Adherent, crack free, but thick.
	(114)	Ce-15% Ni-9% Co	800	75	320	Both layers are uniform, adherent, but contains a few cracks.
<hr/>						
<b>NiCrAlY</b>						
		Ce-18% Ni	650	= 10	= 150	Both outer coating and interaction zones are uniform, adherent, and crack free.
		Ce-18% Co	650	15-40	90-105	Outer coating is not uniform and spalled in a few areas.
	(37)	Ce-30% Ni	700	15-20	= 100	Interaction zone is uniform, adherent, and crack-free..
	(16)	Ce-25% Co	800	No interface, total thickness 1e = 580		Both layers are adherent and crack-free. Uniform, adherent, and crack-free.
<hr/>						
<b>NiCr-1509</b>						
		Ce-18% Ni	650	50-80	= 100	Both outer coating and interaction zone are not uniform, broken and spalled from several areas.
		Ce-18% Co	650	25-50	= 115	Both outer coating and interaction zones are not uniform and contain cracks.
	(10)	Ce-30% Ni	850	30-40	90-110	Both outer coating and interaction zone are not uniform and contain few cracks.
	(123)	Ce-30% Ni	800	Overall thickness = 180-240		Adherent and crack-free.
	(115)	Ce-25% Co	800	25-25	220	Both layers are adherent and crack-free.
	(80)	Ce-15% Ni-9% Co	800	Overall thickness = 270		Uniform, adherent and crack-free.
<hr/>						
<b>CoCrAlY</b>						
		Ce-18% Ni	650	14-12	100-120	Both coating and interaction zones are uniform, adherent, and crack free.
		Ce-18% Co	650	28-35	= 170	Outer coating is not uniform and shows limited spalling.
	(11)	Ce-30% Ni	850	= 20	= 115	Interaction zone is uniform, adherent, and crack-free.
	(93a)	Ce-25% Co	800	Overall thickness = 270		Both layers are uniform, adherent, and crack-free. Uniform, adherent and crack-free.



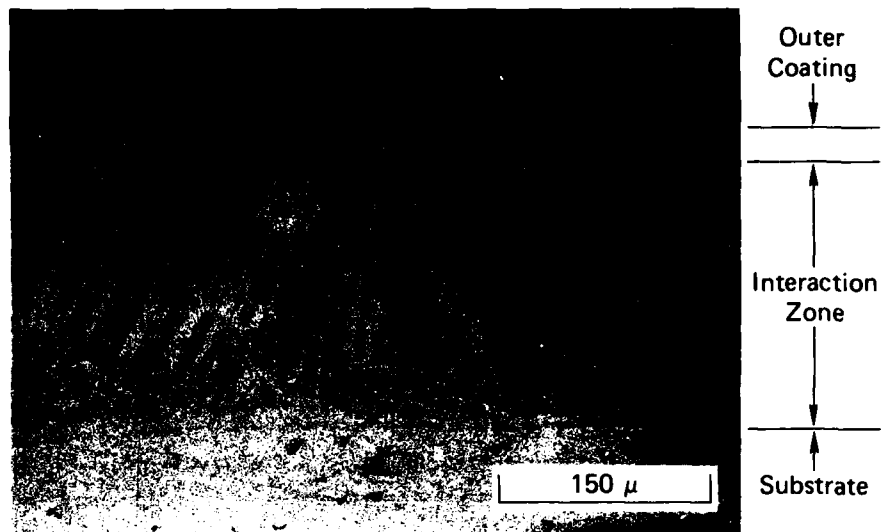
(a) MAR-M509



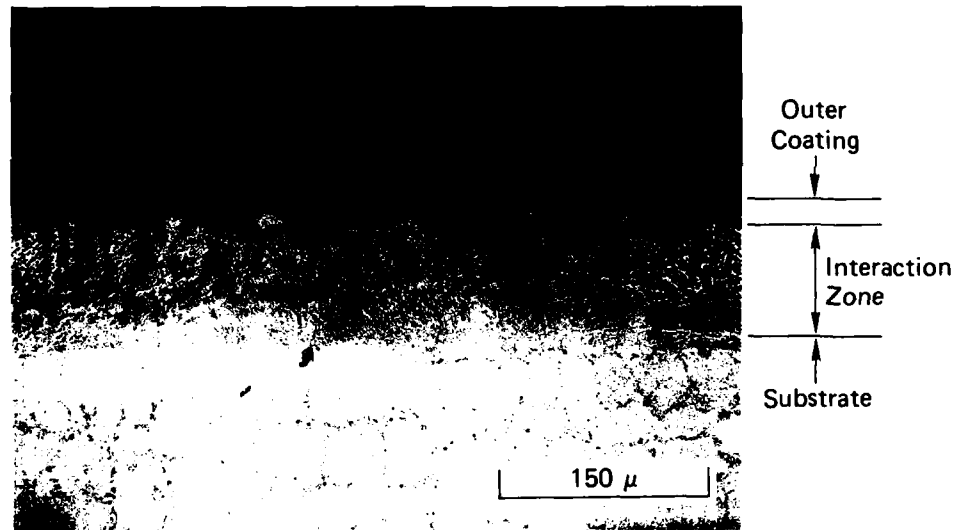
(b) Co-25Cr-6Al-0.5Hf

JP-350583-81

FIGURE 4 CROSS SECTIONS OF ALLOY SUBSTRATES AFTER HOT-DIPPING  
IN Ce-30% Ni



(a) IN-738



(b) Ni-25 Cr-8 Al-1 Y

JP-2509-4

FIGURE 5 CROSS SECTIONS AFTER HOT-DIPPING IN Ce-30 % Ni

- (a) Hot-dipped at 850°C
- (b) Hot-dipped at 700°C

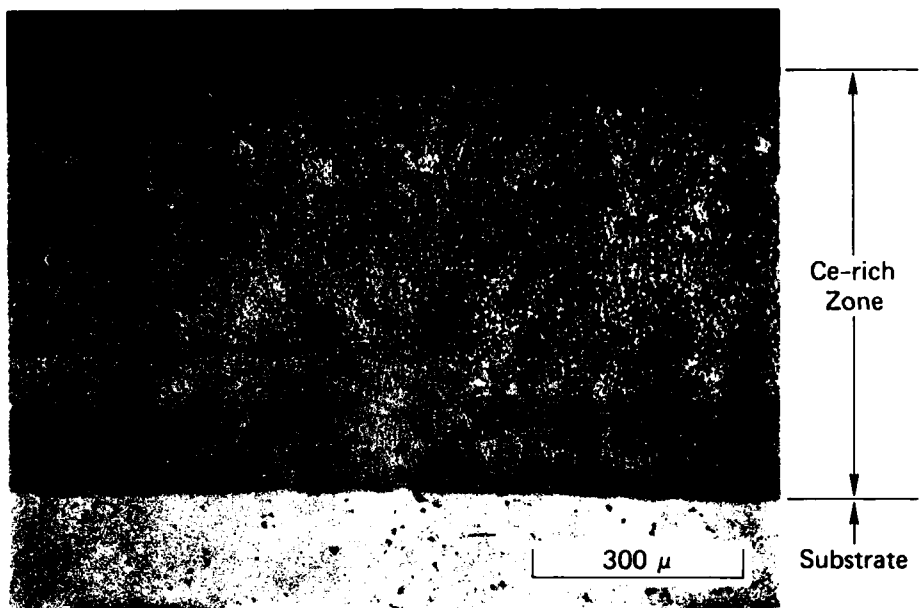
**Table 4**  
**CONDITIONS AND RESULTS OF ANNEALING**

Substrate IN738 27	Sample Number	Dip Temperature (°C)	Annealing Conditions			Overall Coating Thickness (μm)	Results
			Temperature (°C)	Duration (hr)	Thickness (μm)		
	24	850	700	15	400	Uniform, adherent and contains a few small cracks	
			Then redipped at 850 for 30 sec.				
NiCrAlY	30	850	900	4	1300-1350	Adherent, but contains numerous large cracks perpendicular to interface.	
	35	800	800	1	450	Adherent, contains a few cracks.	
MAR M509	28	850	900	4	250	Highly adherent, uniform in thickness, and crack free.	
	152	750	900	3	175-200	Highly adherent, uniform in thickness, and crack free.	
	153	720	900	15	~ 115	Highly adherent, uniform in thickness and crack free	
CoCrAlIn	32	850	900	4	~ 320	Adherent, crack free, but irregular outer surface.	
	78A	850	1000 then at 1050	1-1/2	~ 380	Adherent, crack free, but irregular outer surface.	

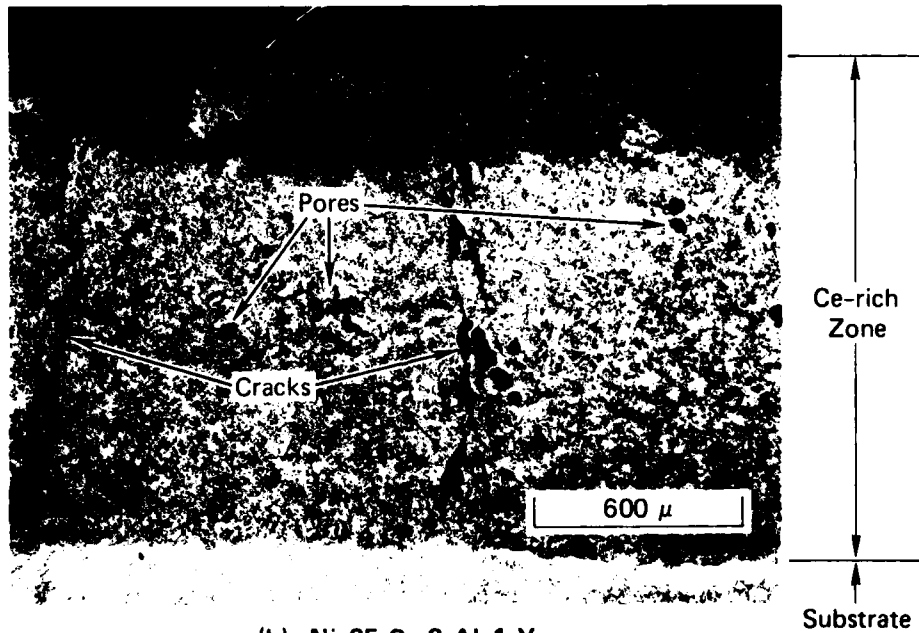
The coating quality after the annealing treatment is evaluated by its thickness, uniformity, cohesion and adhesion to the substrate alloy. Optimization of processing parameters in the first and second steps (hot-dipping and annealing) is directed towards developing a uniform, thin, adherent coating layer. Table 4 indicates that the cerium-rich layer formed on the alloy IN738 is adherent and uniform (but may contain a few cracks), and is relatively thick. Figure 6 shows typical cross sections of the alloys IN738 and NiCrAlY after dipping and annealing. Annealing the hot-dipped NiCrAlY substrate markedly increased the interaction zone thickness, and resulted in the development of large cracks perpendicular to the interface.

In contrast, for the cobalt-base alloys, annealing markedly improved the integrity of the coatings. Under the same annealing conditions, the overall thickness of the cerium-containing layer on the cobalt-base substrate was substantially smaller than that on both nickel-base substrates.

In situ x-ray diffraction analysis of annealed MAR-M509 coated with Ce-30% Ni indicated the presence of metallic cobalt, metallic nickel, and the intermetallics CeNi<sub>3</sub> and CeCo<sub>2</sub> at the external surface. A significant concentration of cobalt at the substrate surface possibly results from outward diffusion from the substrate across the Ce-rich zone. Figure 7 shows the concentration profiles of Ce, Co, Ni and Cr across the coating layer on the alloy MAR-M509 after hot dipping in Ce-30% Ni then annealing at 900°C for 15 h. The outer portion of the coating layer is rich in cerium, and the cerium concentration drops gradually towards the alloy substrate. Cobalt has an opposite concentration gradient to cerium, however, its concentration remains relatively high at the gas/coating interface. The large light particles in the middle zone of the coating layer appear to contain neither cerium nor cobalt. They are rich in chromium and contain only a small quantity of nickel. The nickel concentrations appear to be constant across the coating and almost equal to that of the alloy substrate ( $\approx 10\%$ ). The inner portion of the coating, near the unaffected substrate is rich in chromium, whose concentration drops sharply within the outer portion of the coating.



(a) IN-738



(b) Ni-25 Cr-8 Al-1 Y

JP-2509-5

FIGURE 6 CROSS SECTIONS OF NICKEL-BASE SUBSTRATES AFTER HOT-DIPPING IN Ce-30% Ni AT 850°C FOLLOWED BY ANNEALING IN PURE ARGON AT 900°C FOR 4 HOURS

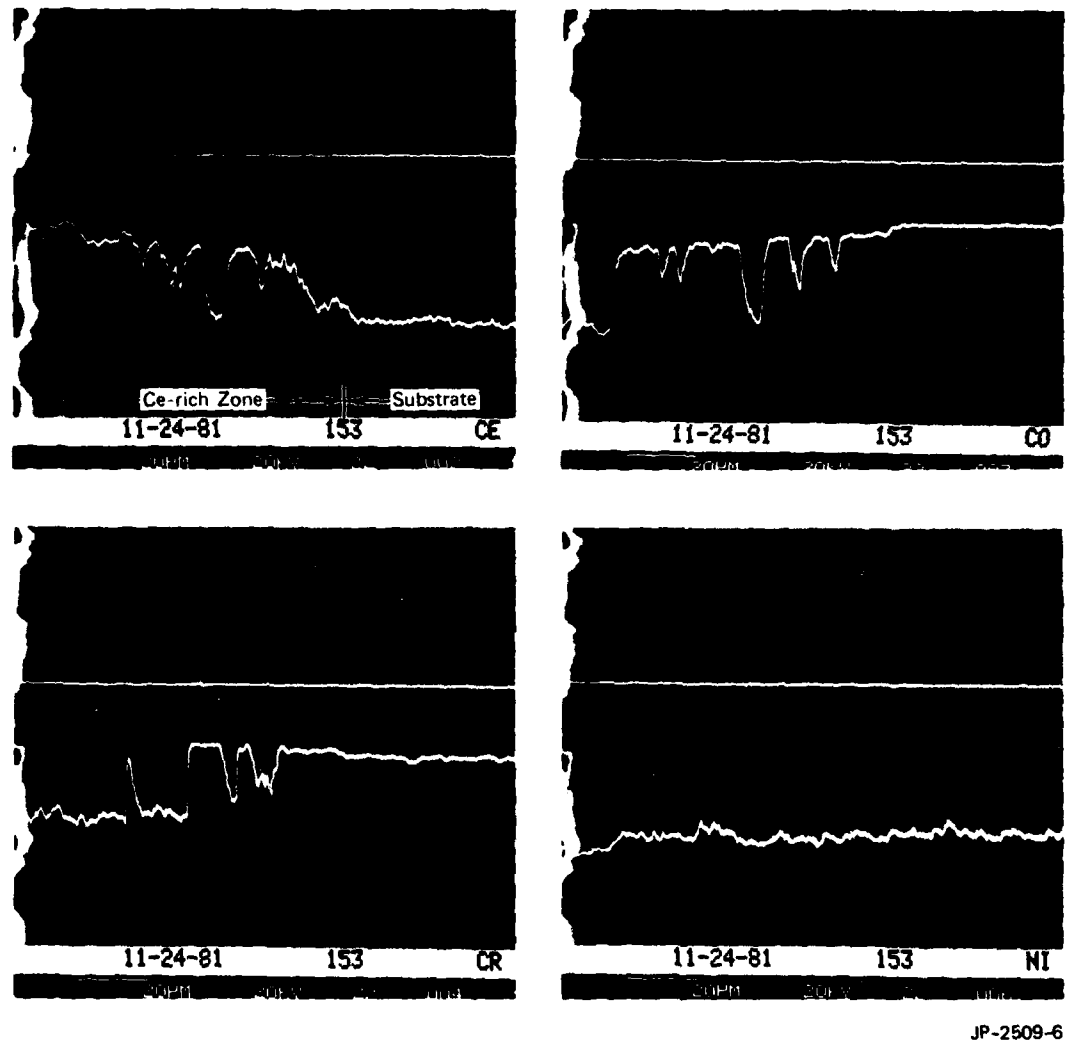


FIGURE 7 CONCENTRATION PROFILES SHOWING THE DISTRIBUTION OF Ce, Co, Cr AND Ni ACROSS COATED ALLOY SUBSTRATE MAR-M509 FOLLOWING HOT-DIPPING IN Ce-30 % Ni AT 720°C AND ANNEALING AT 900°C FOR 15 HOURS

Annealing the coated CoCrAlHf alloy results in a thicker interaction zone compared with MAR-M509, probably due to faster inward diffusion of cerium (Table 4). The major feature of this alloy is the highly irregular morphology of the coating surface and the presence of numerous chromium-rich second phase particles within the outer portion of the coating layer, Figure 8.

#### C. Internal Oxidation

The results of the internal oxidation treatment of coated substrates after hot-dipping and annealing are presented in Table 5. Optimizing the processing conditions during hot-dipping, annealing, and internal oxidation resulted in the development of thin, uniform and highly adherent duplex coatings on the cobalt-base substrates, particularly MAR-M509. The improvement of coating quality on these substrates seems to be associated with the limited coating/substrate interdiffusion and the absence of microstructural defects, such as porosity and microcracks.

In contrast, optimizing the processing conditions for coatings on both nickel-base alloys was less successful. Extensive coating/substrate interdiffusion during hot-dipping and annealing leads to excessive thickening of the cerium-rich layer at the substrate surface and the development of porosity and extensive cracking. Further internal oxidation allows oxygen permeation through these defects across the coating and leads to the development of thick and nonprotective oxide scales.

These results, as summarized in Table 5, clearly indicate that the coatings on MAR-M509 had the greatest integrity and that this alloy coated with Ce-30% Ni showed the best promise for further optimization. Therefore, this system was chosen as a model for a more intensive study of the factors affecting coating morphology, composition and properties. Details of the microstructures of internally oxidized coatings on the four superalloy substrates are described in the following subsections.

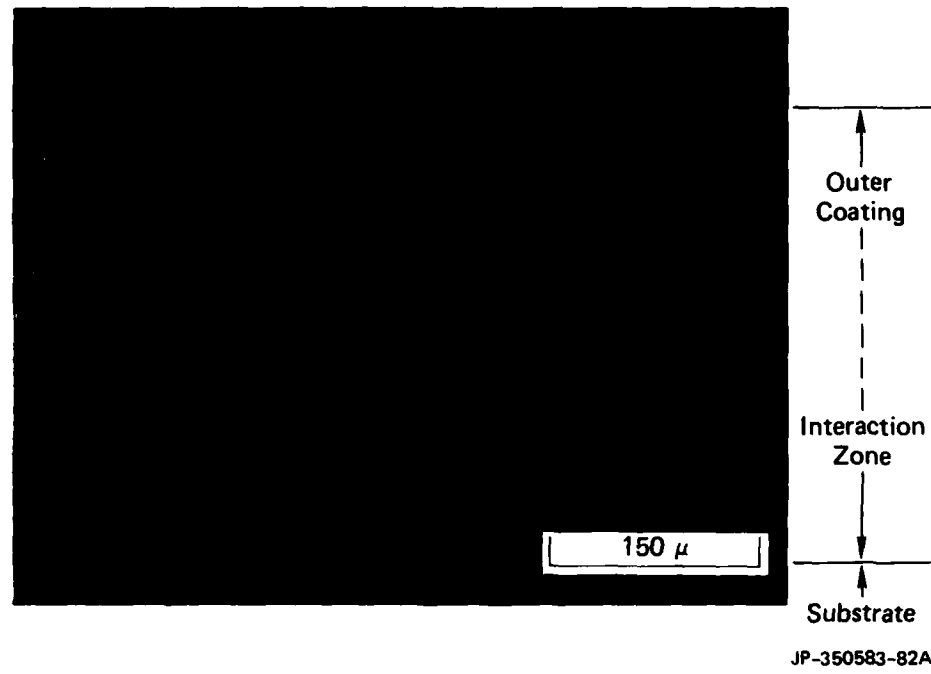


FIGURE 8 CROSS SECTION OF ALLOY SUBSTRATE Co-25 Cr-6 Al-0.5 Hf AFTER HOT-DIPPING AND ANNEALING AT 900°C FOR 4 HOURS

## CONDITIONS AND RESULTS OF INTERNAL OXIDATION

Alloy Number	Sample Number	Annealing Temperature (°C)	Annealing Time (hr)	1. Oxidation		Post 1. Oxidation Temperature (°C)	Post 1. Oxidation Time (hr)	Oxide Thickness (μm)	Remarks
				Temperature (°C)	Time (hr)				
MAN M509	2A	Ce-30% Ni at 850°C	900	4	600	44	800	28	Uniform, adherent, no cracks.
	148	Ce-30% Ni at 800°C	900	1	588	45	800	24	Uniform, adherent, no cracks.
	92	Ce-30% Ni at 750°C	800	2	600	48	700	2	Uniform, adherent, no cracks. Then annealed at 700°C for 16 hours.
	88	Ce-15% Ni-9% Co at 800°C	850 other 940	2	600	44	800	22	Extensive cracking and spallation. and redipped at 850°C for 10 sec
<hr/>									
CuCrAlN	31A	Ce-30% Ni at 850°C	900	4	600	44	800	28	Adherent, uniform, contains cracks at corners, outer surface is highly irregular.
	58	Ce-30% Ni at 750°C	800	4	575	24	800	20	Uniform, horizontal cracks along coating/substrate interface.
	72	Ce-30% Ni at 750°C	900	4	575	45	800	20	Uniform, fairly adherent, contains cracks parallel to coating/substrate interface.
	76B	Ce-30% Ni at 850°C	1000	1-1/2	600	44	800	20	Uniform, adherent, few corner cracks.
	99B	Ce-25% Co at 800°C	-	-	1050	1	-	-	Spallation extensive.
	1073B	27A	Ce-30% Ni at 850°C	900	4	600	44	800	28
	100	Ce-25% Co at 800°C	-	-	590	70	700	4	Extensive porosity and complete spallation.
	90B	Ce-75% Ni-9% Co at 800°C	80	1/2	590	70	700	4	Extensive porosity and spallation.
	70	Ce-30% Ni at 750°C	800	2	577	45	800	20	Incomplete oxidation of Ce. Extensive spallation.
<hr/>									
HGSAlN	29A	Ce-30% Ni at 850°C	900	4	600	44	800	28	Extensive cracking and spallation.
	34	Ce-30% Ni at 800°C	800	1	600	90	-	28	Incomplete oxidation of Ce, extensive cracking.
	70	Ce-30% Ni at 750°C	800	2	577	45	800	20	Adherent, fairly uniform, contains corner cracks.

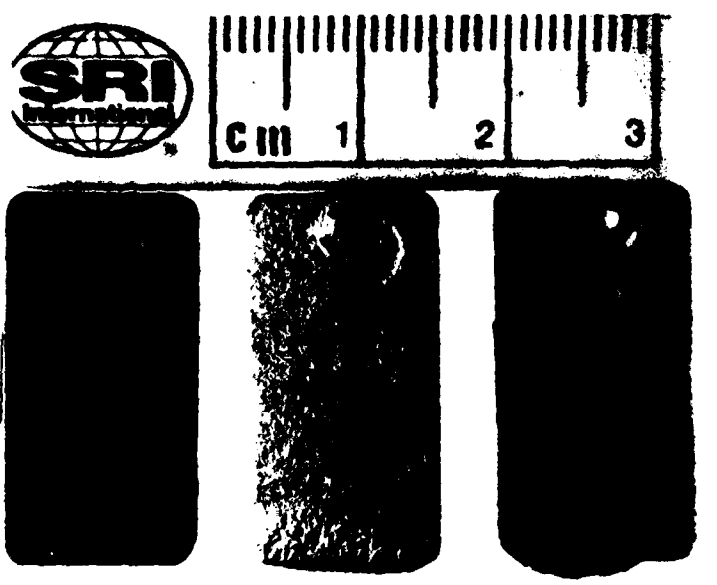
### 1. MAR-M509

The oxide layer formed on MAR-M509 was fairly thin, uniform, adherent and crack free, and exhibited the duplex configuration of an outer continuous oxide above an inner-composite subscale. Figure 9 shows the surface morphologies of MAR-M509 coupons. The microstructure of the coating on the substrate MAR-M509 is presented in Fig. 10. A thin, semicontinuous metallic layer, very rich in nickel and cobalt, forms during the internal oxidation treatment at the oxide/gas interface. The outer portion of the subscale layer consists of an oxide matrix ( $CeO_2$ ) containing a large number of metallic islands. Near the coating substrate interface, the subscale structure consists of thin fibrous oxide lamellae embedded into the metallic substrate.

Figure 11 shows the concentration profiles of different elements across the oxide layer of the sample shown in Fig. 10. The outer metallic semicontinuous layer is composed almost exclusively of nickel and cobalt and contains small concentrations of cerium and chromium. The continuous external oxide layer (thermal barrier) was very rich in cerium in the form of  $CeO_2$ ; however, it contained high concentrations of nickel and cobalt. Within the subscale zone, the profiles of nickel and cobalt were almost identical and both were often opposite to that of chromium. Tungsten exists mainly in the discrete second phase particles in the substrate alloy.

It appears that the outer portion of the subscale layer consists of a cerium oxide ( $CeO_2$ ) matrix that contains high nickel and cobalt concentrations. The large metallic islands embedded in this oxide matrix are very rich in chromium and almost coincide with the Cr-rich islands produced by annealing (Fig. 7). Identification of individual phases of the fibrous microstructure within the inner subscale portion near the substrate was not possible because of the fine submicron size particles. However, the analysis indicates that this area consists of cerium oxide embedded in a metallic matrix of a composition similar to that of the substrate.

In a multicomponent system, where only one component can oxidize, two possible conditions exist:



JP-2509-7

FIGURE 9 SURFACE MORPHOLOGIES OF THE ALLOY MAR-M509

From left to right: Uncoated; hot-dipped in Ce-30% Ni at 800°C, then annealed at 900°C for 3 hours; hot-dipped at 800°C and annealed at 900°C for 3 hours, then internally oxidized at 588°C for 45 hours followed by further internal oxidation at 800°C for 24 hours.

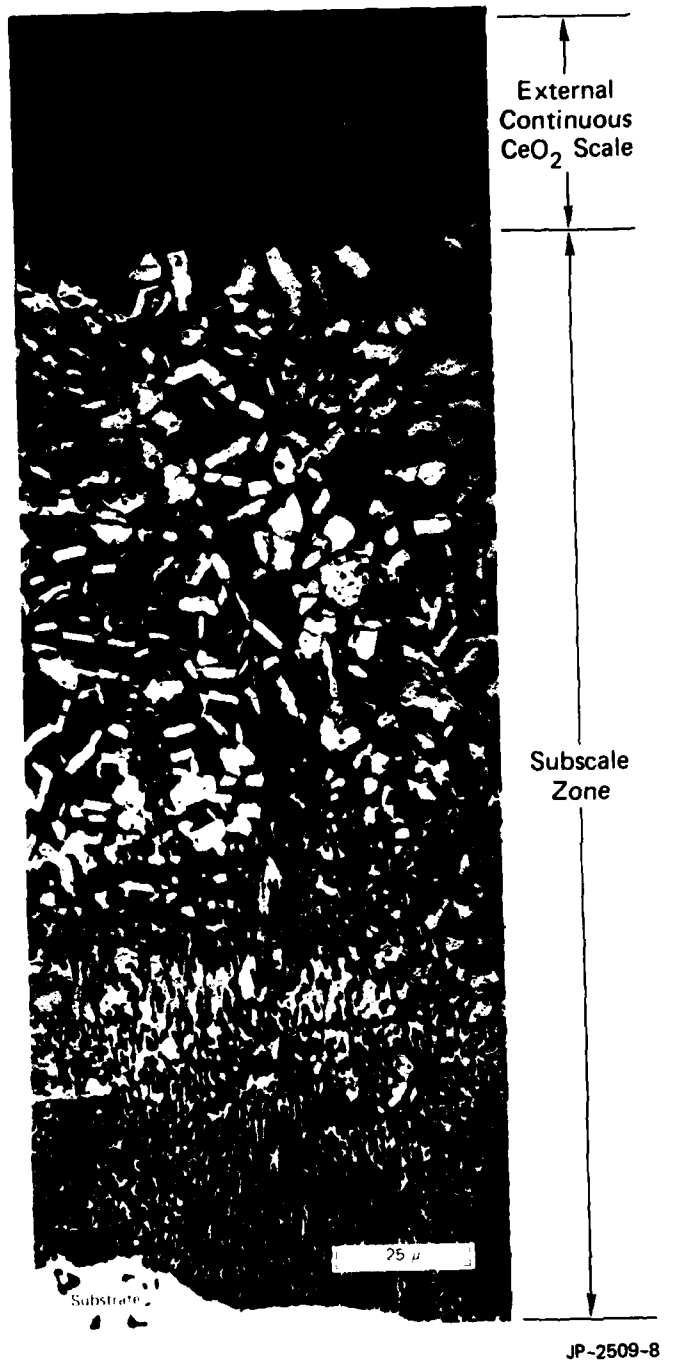


**FIGURE 10 CROSS SECTION OF COATED MAR-M509**  
Hot-dipped in Ce-30% Ni at  $800^\circ\text{C}$ , annealed at  $900^\circ\text{C}$  for 3 hours, then internally oxidized at  $588^\circ\text{C}$  for 45 hours followed by further internal oxidation at  $800^\circ\text{C}$  for 24 hours.

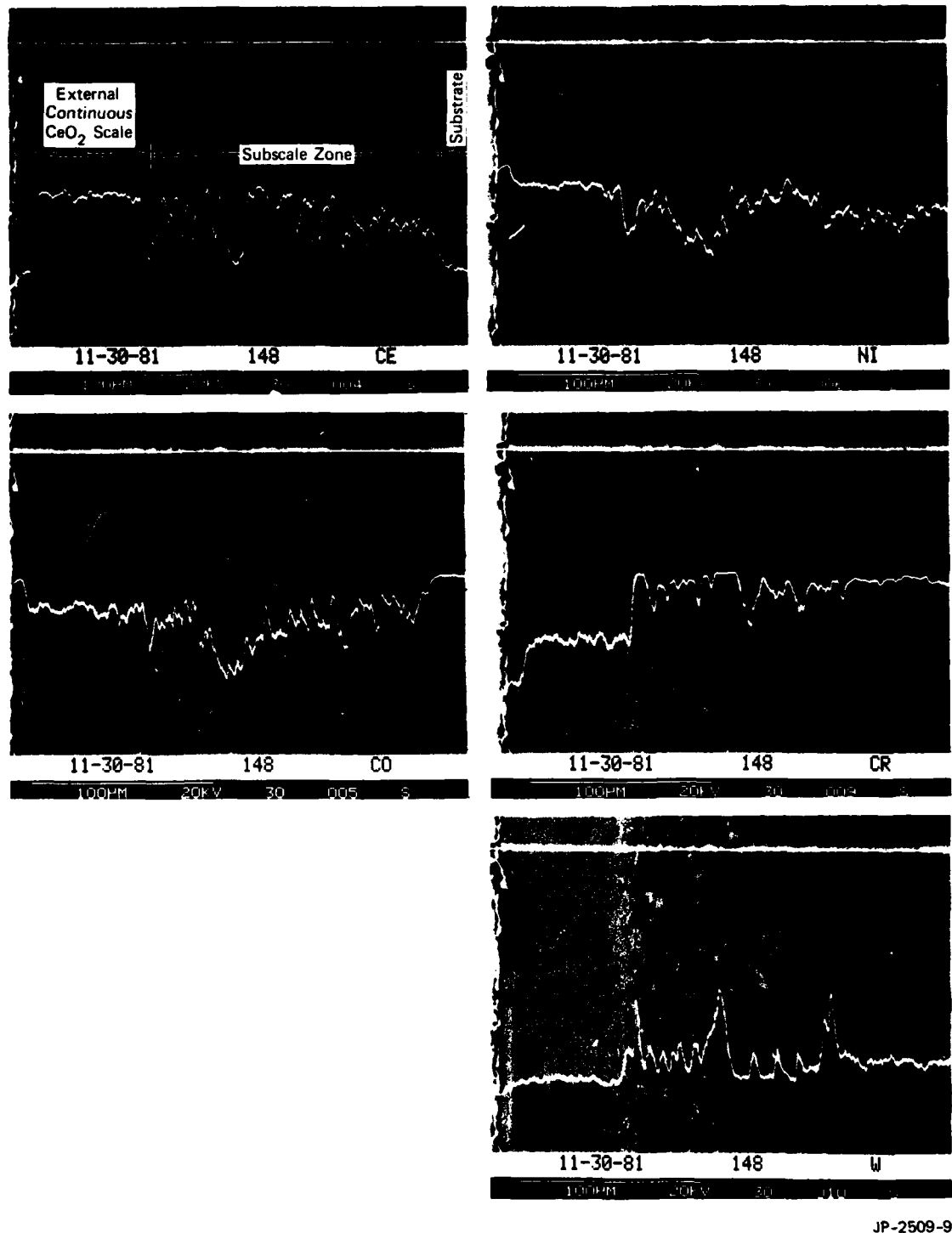


FIGURE 11 CONCENTRATION PROFILES OF Ce, Ni, Co, Cr, AND W ACROSS COATED MAR-M509 SPECIMEN SHOWN IN FIGURE 10

- (1) If the oxide growth rate is slow (for example  $\text{Al}_2\text{O}_3$  or  $\text{Cr}_2\text{O}_3$ ), then a concentration gradient of remaining metals will be established in the alloy substrate ahead of the interface. The highest concentrations will obviously exist at the oxide/substrate interface. This gradient acts as a driving force for back diffusion of these elements into the substrate away from the oxide. The oxide in this case will not incorporate the unoxidized metal because its slow growth rate allows ample time for the back diffusion of these elements.
- (2) If the oxide growth rate is fast (for example, rare earths), then the back diffusion of the unoxidized elements will be overrun by the rapid inward growth of the interface. Under this condition, the growing oxide will probably incorporate fairly high levels of the unoxidized metals.

The latter condition appears to represent the pattern followed during the internal oxidation treatment of the present systems. Because of the high thermodynamic stability of cerium oxide, no other oxide ( $\text{NiO}$ ,  $\text{CoO}$ , and  $\text{Cr}_2\text{O}_3$ ) is expected to form. As cerium oxide forms an external continuous scale during the internal oxidation treatment, the ingressing oxide/alloy interface will incorporate other metallic constituents whose oxides would not form because of the low oxygen activity.

The nickel- and cobalt-rich islands at the gas/oxide interface were probably formed during the initial stages of oxidation. This is confirmed by the minimal change in their thickness after exposure for extended periods. The presence of these islands is possibly a result of the preferential nucleation and growth of cerium oxide ( $\text{CeO}_2$ ) as discrete particles during the very early stages of oxidation. The areas between these particles will be poorer in cerium and richer in nickel and cobalt. Further oxidation will lead to the inward and lateral growth of cerium oxide nuclei, thus undercutting these metallic islands from the alloy substrate.

Semiquantitative in-situ x-ray analysis of the oxide layer formed by internal oxidation was conducted along planes parallel to the interface and at different depths from the external surface. At the outer surface of the coated sample, the concentrations of cobalt and nickel were estimated at about 90 wt% with the remaining portion being cerium oxide ( $\text{CeO}_2$ ). At a

depth of 30  $\mu\text{m}$  below the outer surface (middle of external continuous oxide layer), The analysis indicates that the  $\text{CeO}_2$  concentration rise to about 30 wt%, while nickel and cobalt concentrations drop to about 70 wt%. At 75  $\mu\text{m}$  depth (outer portions of the subscale layer), the  $\text{CeO}_2$  concentration reaches about 60 wt%. The remaining portion is predominantly nickel and cobalt and a slight amount of chromium. X-ray analysis of a section at 100  $\mu\text{m}$  depth indicates a composition similar to that at 75  $\mu\text{m}$  depth. These results are in fair agreement with the concentration profiles shown in Figure 11.

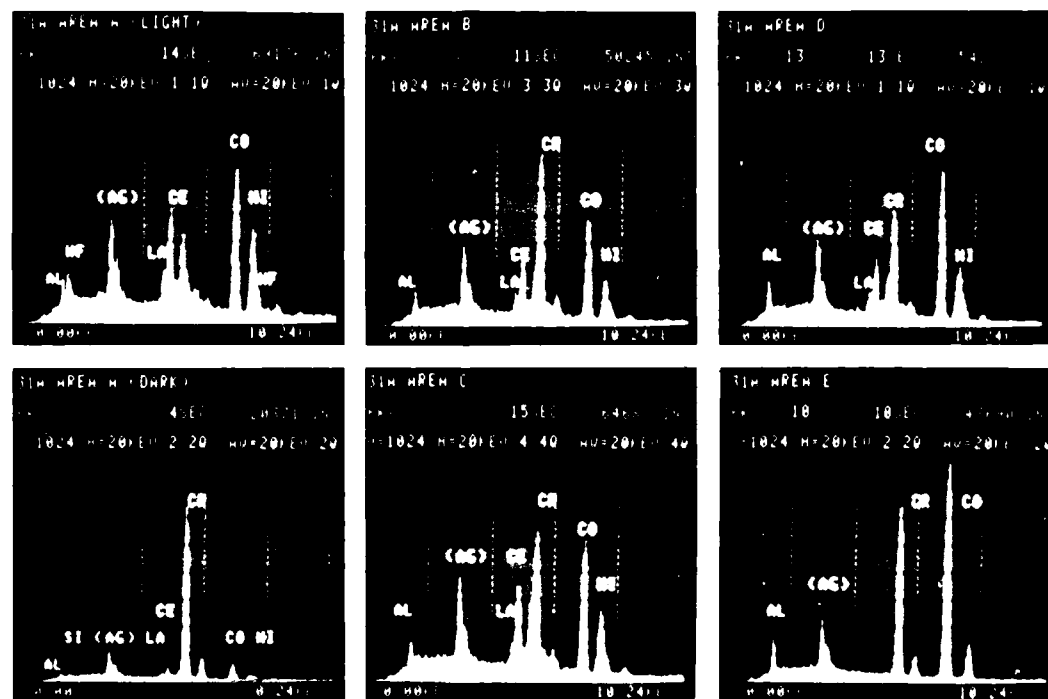
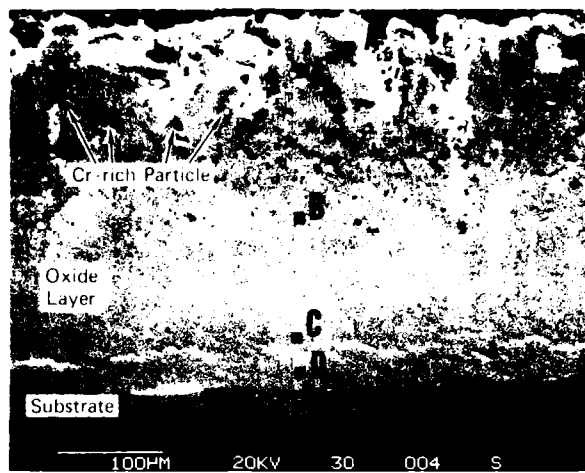
## 2. CoCrAlHf

The microstructure and elemental analysis of the coating formed on the alloy CoCrAlHf is shown in Fig. 12. The overall coating thickness was about 350  $\mu\text{m}$ . The major difference between this coating and that formed on the similarly treated MAR-M509 alloy, was that this coating had no external continuous cerium oxide layer. In addition, the large chromium-rich islands appear to concentrate in the outer portion of the coating, particularly at the highly irregular gas/coating interface. In general, this coating appears to be less promising than the coating on MAR-M509, (Figure 10) because:

- (1) This coating is one-third thicker than that in MAR-M509.
- (2) There is no outer continuous cerium oxide layer that is useful as a thermal barrier.
- (3) The coating is less adherent than on MAR-M509.

## 3. Nickel-Base Alloys

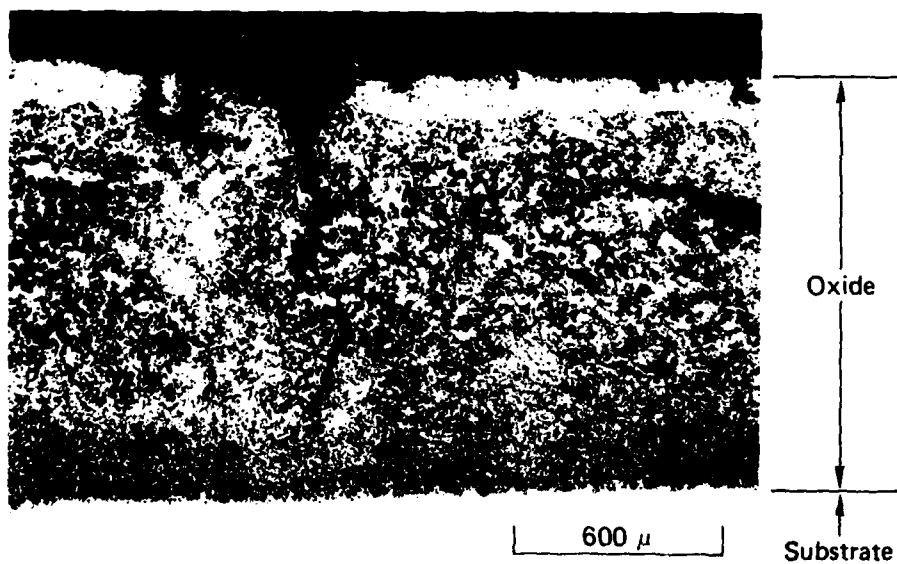
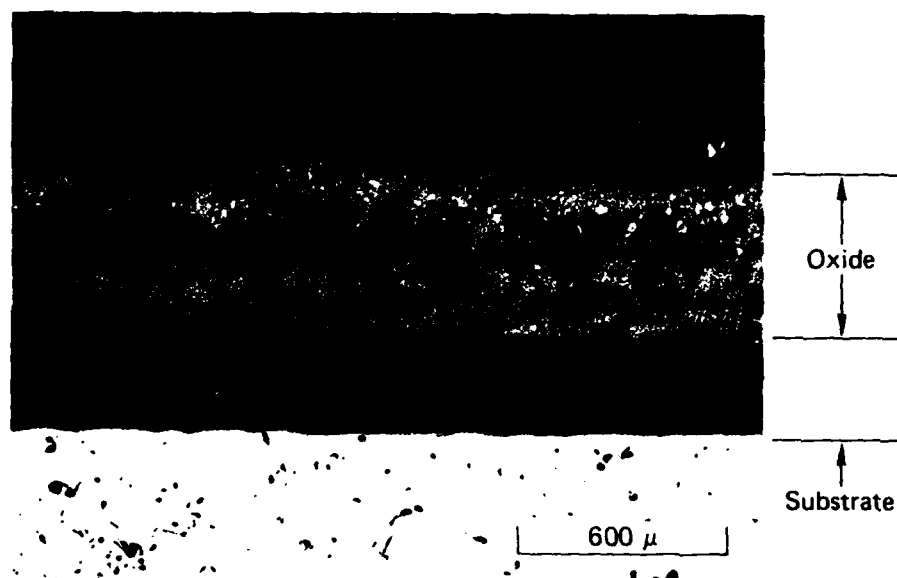
Figure 13 shows typical cross sections of the coated substrates IN738 and NiCrAlY. The coatings on both alloys are very thick, porous and contain large cracks. The coatings spalled extensively upon cooling both alloys from the internal oxidation temperature. Changes in the conditions of hot-dipping, annealing and internal oxidation treatments did not produce any significant improvement in the coating integrity. Microstructural analysis of coated substrates indicated the absence of the external cerium



JP-2509-10

**FIGURE 12 MICROSTRUCTURE AND ANALYSIS OF COATED Co-25 Cr-6 Al-0.5 Hf**

Hot-dipped in Ce-30 % Ni at 850°C, annealed at 900°C for 4 hours, and internally oxidized at 600°C for 44 hours followed by further internal oxidation at 800°C for 28 hours.



JP-2509-11

FIGURE 13 CROSS SECTIONS OF ALLOY SUBSTRATES

Hot-dipped in Ce-30 % Ni at 850°C, annealed at 900°C for 4 hours,  
then internally oxidized at 600°C for 44 hours followed by further  
internal oxidation at 800°C for 28 hours.

oxide layer at the coating surface. Ce, Cr, and Ni exist at constant levels across the coating. No further analysis was performed on the alloys.

#### D. Recrystallization Annealing

Figure 14 shows the microstructure of coated MAR-M509 after completing the four-step process. The sample was dipped in Ce-30% Ni at 750°C, annealed for 15 h at 900°C, oxidized in CO/CO<sub>2</sub> for 67 h at 600°C then for 20 h at 800°C. Finally, it was annealed in pure argon for 5 h at 950°C. The overall coating thickness was  $\approx$  170  $\mu\text{m}$ , of which the outer continuous oxide layer is  $\approx$  35  $\mu\text{m}$ . In comparison with samples that did not receive the crystallization annealing treatments, (Fig. 10), no significant differences in the coating morphology resulted from the final treatment. The large metallic islands in the middle portion of the coating (outer portion of the subscale) in the recrystallized sample (Fig. 14) were produced during the long vacuum annealing (15 h) before internal oxidation.

Figure 15 shows the concentration profiles of different elements across the coating in MAR-M509 sample that received the complete four-step treatment. The outer continuous oxide layer contains the highest concentration of cerium, which drops gradually across the subscale layer towards the substrate. The large metallic islands within the subscale zone are very rich in chromium but contain very little cerium, cobalt, and nickel.

Unlike the profiles for the nonrecrystallized sample shown in Fig. 11, where cobalt and nickel concentrations are almost constant across the external continuous oxide layer, the concentrations of both elements appear to drop towards the subscale. On the other hand, the chromium concentration seems to rise steeply in the opposite direction, and remains at a high level, within the subscale zone. As with the nonrecrystallized coating (Fig. 11), the external surface of the coating on the recrystallized sample (Figure 14) is covered with a Ni/Co metallic layer. In-situ x-ray diffraction analysis of the sample shown in Fig. 15 indicates that the composition of the outer surface (gas/coating interface) is about 80-85 wt% cobalt and nickel, 10-15 wt% Ce<sub>2</sub>O<sub>3</sub> and the remaining phase ( $\approx$  5%) conforms to the

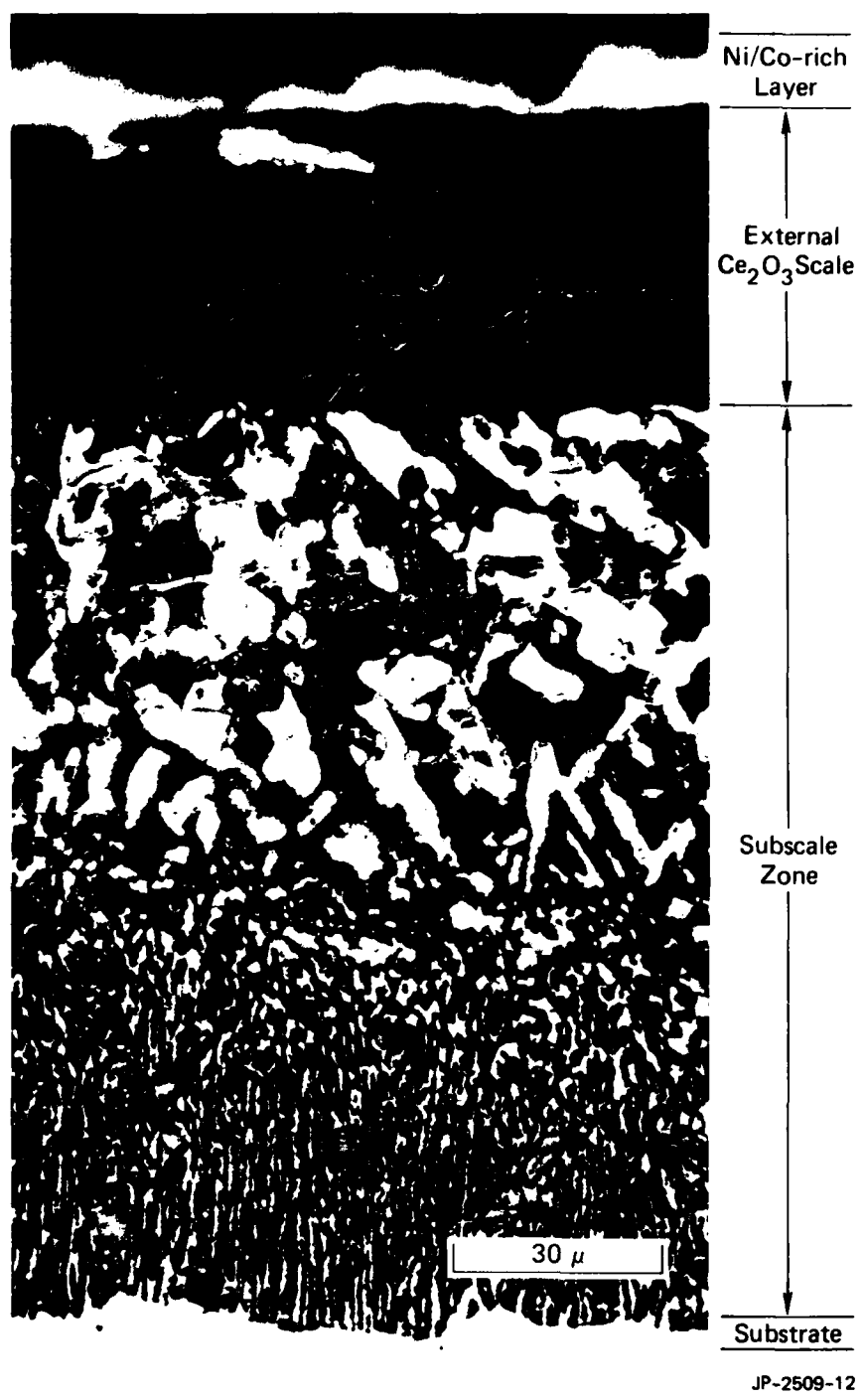
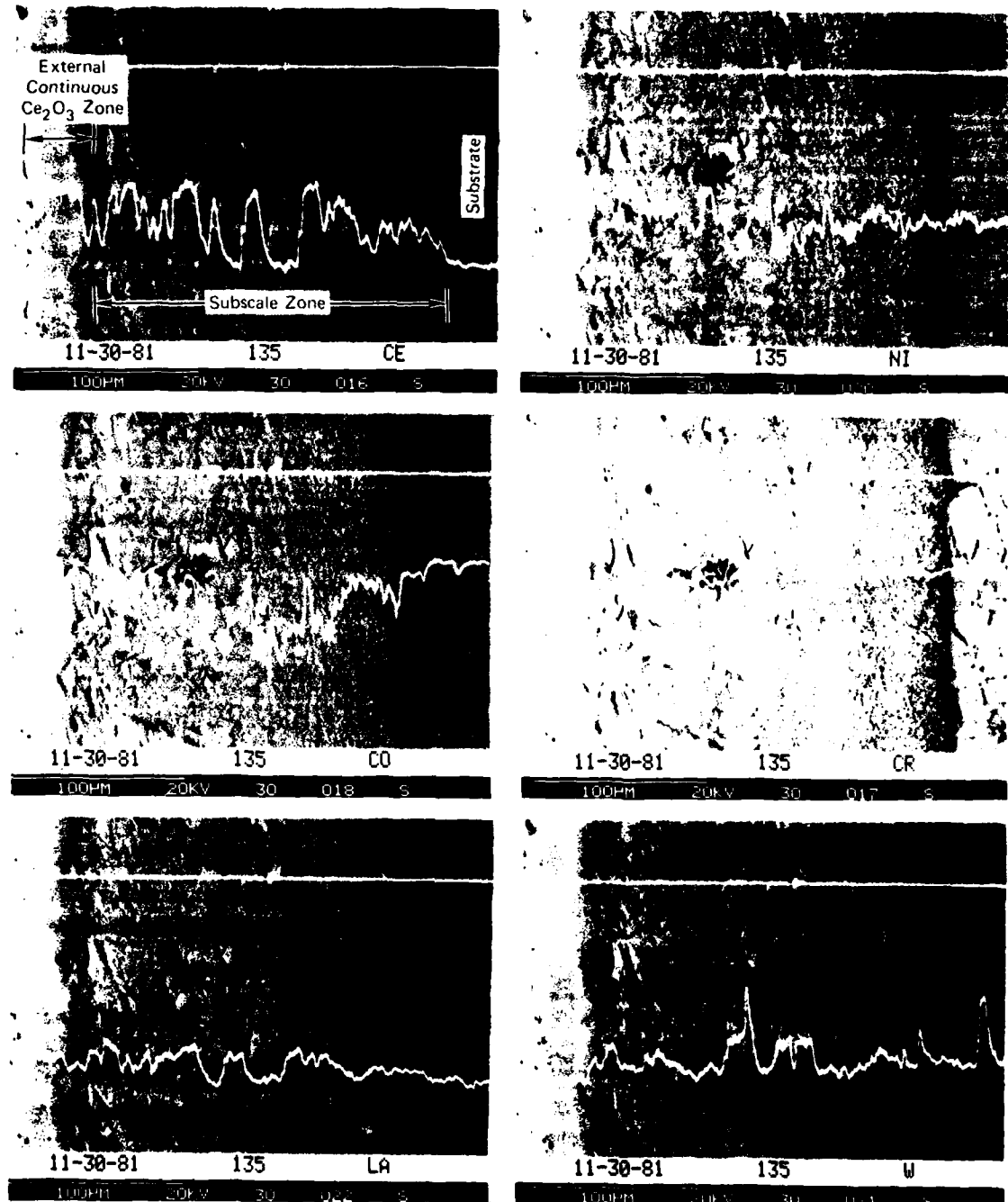


FIGURE 14 CROSS SECTION OF COATED MAR-M509

Hot-dipped in Ce-30 % Ni at 750°C, annealed at 900°C for 15 hours, then internally oxidized at 600°C for 67 hours followed by further internal oxidation at 800°C for 20 hours, and final recrystallization annealing for 5 hours at 950°C.



JP-2509-13

**FIGURE 15 CONCENTRATION PROFILES OF Ce, Ni, Co, Cr, La, AND W ACROSS COATED MAR-M509 SPECIMEN (SHOWN IN FIGURE 14) AFTER RECEIVING FINAL RECRYSTALLIZATION ANNEALING**

cubic compound  $\text{La}_6\text{WO}_{12}$ , where La is a major impurity in the cerium mish-met used in the original coating alloy. Interestingly, the higher cerium oxide ( $\text{CeO}_2$ ) was not present within the coating across the entire cross section of the coating.

At a depth of 15  $\mu\text{m}$  within the external continuous oxide layer the concentration of both nickel and cobalt remains as high as 70 wt%.  $\text{Ce}_2\text{O}_3$  was estimated to be about 10-15 wt% and the cubic  $\text{La}_6\text{WO}_{12}$  phase amounts to 5-10 wt%. At this depth, a new phase (about 10 wt%) conforms to the orthorhombic double oxide  $0.5(\text{La}_2\text{O}_3 \cdot \text{Cr}_2\text{O}_3)$ . Because of the similarity of the atomic diameters of La (1.88 Å) and Ce (1.82 Å), it is possible that lanthanum atoms are partially substituted by cerium atoms in the lattice to form mixed oxides  $0.5(\text{Ce}_2\text{O}_3 \cdot \text{La}_2\text{O}_3 \cdot \text{Cr}_2\text{O}_3)$  and  $(\text{La,Ce})_6\text{WO}_{12}$ . A further reason for this substitution is the abundance of cerium relative to lanthanum, which mainly exists as an impurity in the cerium mish metal. The x-ray pattern of a section at 60  $\mu\text{m}$  below the coating surface showed that the mixed oxide phase  $0.5(\text{La}_2\text{O}_3 \cdot \text{Cr}_2\text{O}_3)$  or  $0.5(\text{Ce}_2\text{O}_3 \cdot \text{La}_2\text{O}_3 \cdot \text{Cr}_2\text{O}_3)$  amounts to 45 wt%, metallic nickel and cobalt amount to about 40%,  $\text{La}_6\text{WO}_{12}$  or  $(\text{La,Ce})_6\text{WO}_{12}$  amounts to  $\approx 10$  wt%, and  $\text{Ce}_2\text{O}_3$  amounts only to  $\approx 5$  wt%. The very broad x-ray peaks in  $\text{Ce}_2\text{O}_3$  in the deeper section suggest that its grain size is extremely small.

The most important result of this analysis is the complete absence of  $\text{CeO}_2$  in the coating on the recrystallized sample. It appears that recrystallization annealing in oxygen free argon at high temperature reduces  $\text{CeO}_2$  to  $\text{Ce}_2\text{O}_3$  according to the reaction:



At equilibrium, the oxygen partial pressure for this reaction is about  $3.3 \times 10^{-19}$  atm. The oxygen partial pressure under the recrystallization annealing condition appears to fall below this value, thus forcing the reduction reaction of  $\text{CeO}_2$ .  $\text{CeO}_2$  is known to be easily reducible to  $\text{Ce}_2\text{O}_3$  at low oxygen pressure.<sup>1</sup> Further solid state reactions are expected to take place during this treatment that can lead to the formation of the

mixed oxides,  $\text{La}_6\text{WO}_{12}$ ,  $(\text{La},\text{Ce})_6\text{WO}_{12}$  and 0.5 ( $\text{La}_2\text{O}_3 \cdot \text{Cr}_2\text{O}_3$ ) or 0.5 ( $\text{CeO}_2 \cdot \text{La}_2\text{O}_3 \cdot \text{Cr}_2\text{O}_3$ ).

It is highly unlikely from a thermodynamic standpoint that further reduction of the sesquioxide to metallic cerium can occur:

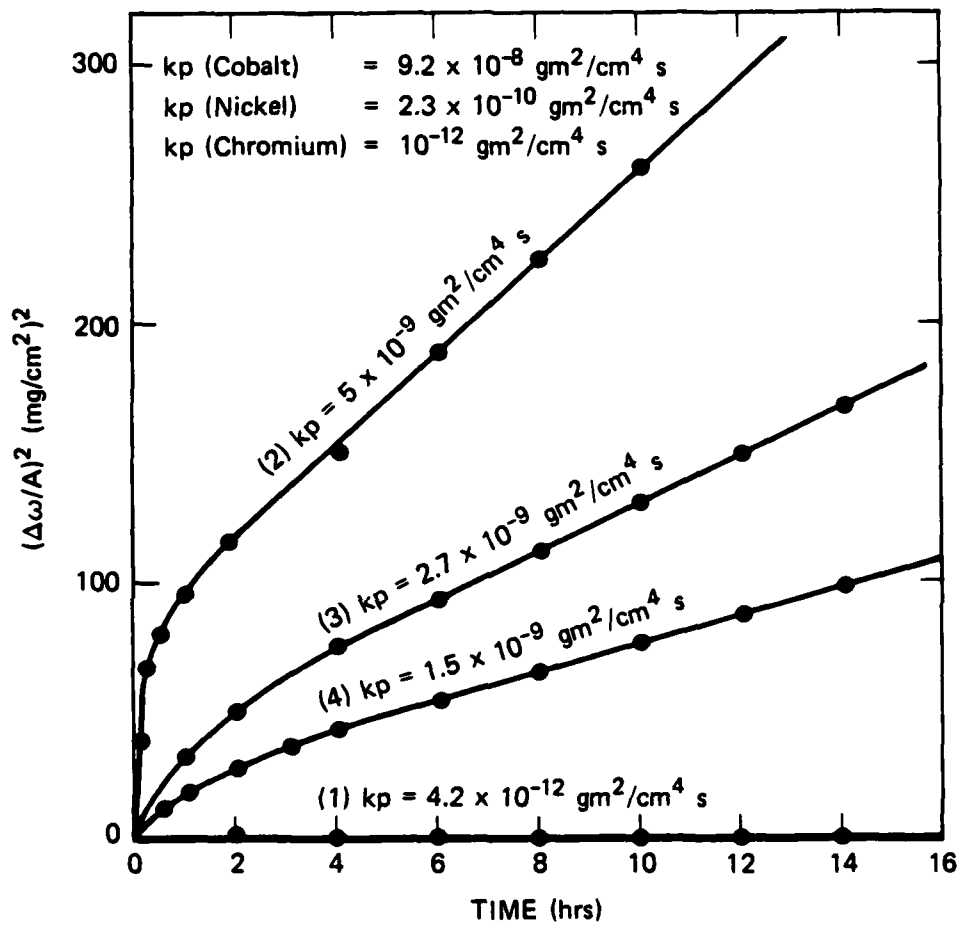


At  $900^\circ\text{C}$  (recrystallization temperature), the equilibrium  $P_{\text{O}_2}$  for this reaction is about  $2.45 \times 10^{-44}$  atm, which is unattainable under these experimental conditions.

#### E. Evaluation

Figure 16 shows an isothermal weight gain versus time plot for uncoated and coated MAR-M509 samples oxidized in oxygen ( $P_{\text{O}_2} = 150$  torr) at  $936^\circ\text{C}$  monitored with a continuous recording microbalance. The uncoated sample (curve 1) showed a very short transient stage, of about 10 min, followed by parabolic growth with a rate constant of  $k_p = 4.2 \times 10^{-12}$   $\text{gm}^2/\text{cm}^4 \text{ sec}$ , that is in fair agreement with the reported value of  $k_p$  for  $\text{Cr}_2\text{O}_3$  ( $\approx 10^{-12}$   $\text{gm}^2/\text{cm}^4 \text{ sec}$ ).<sup>18</sup> The scale is exclusively  $\text{Cr}_2\text{O}_3$  and highly adherent during exposure but partially spalls during cooling. Curve 2 shows the kinetic behavior of a coated MAR-M509 sample. The coating conditions include hot-dipping in Ce-30% Ni at  $720^\circ\text{C}$ , annealing for 15 h at  $900^\circ\text{C}$ , then internal oxidation in a  $\text{CO}/\text{CO}_2$  mixture for 45 h at  $600^\circ\text{C}$ . This is followed by further internal oxidation in  $\text{CO}/\text{CO}_2$  for 25 h at  $800^\circ\text{C}$ , but received no recrystallization annealing treatment. The transient stage of all coated samples averages between 2 to 3 h, followed by a parabolic growth.

The parabolic rate constant for the oxidation of the coated sample shown in curve 2 is about  $5 \times 10^{-9}$   $\text{gm}^2/\text{cm}^4 \text{ sec}$ , almost three orders of magnitude higher than that of the uncoated alloy shown in curve 1 ( $\approx 4.2 \times 10^{-12}$   $\text{gm}^2/\text{cm}^4 \text{ sec}$ ). The value of the parabolic rate constant for curve 2 ( $5 \times 10^{-9}$   $\text{gm}^2/\text{cm}^4 \text{ sec}$ ) approximates an intermediate value between  $k_p$  for cobalt oxide ( $9.2 \times 10^{-8}$   $\text{gm}^2/\text{cm}^4 \text{ sec}$ ) and  $k_p$  for nickel oxide ( $2.3 \times 10^{-10}$   $\text{gm}^2/\text{cm}^4 \text{ sec}$ ).<sup>18</sup>



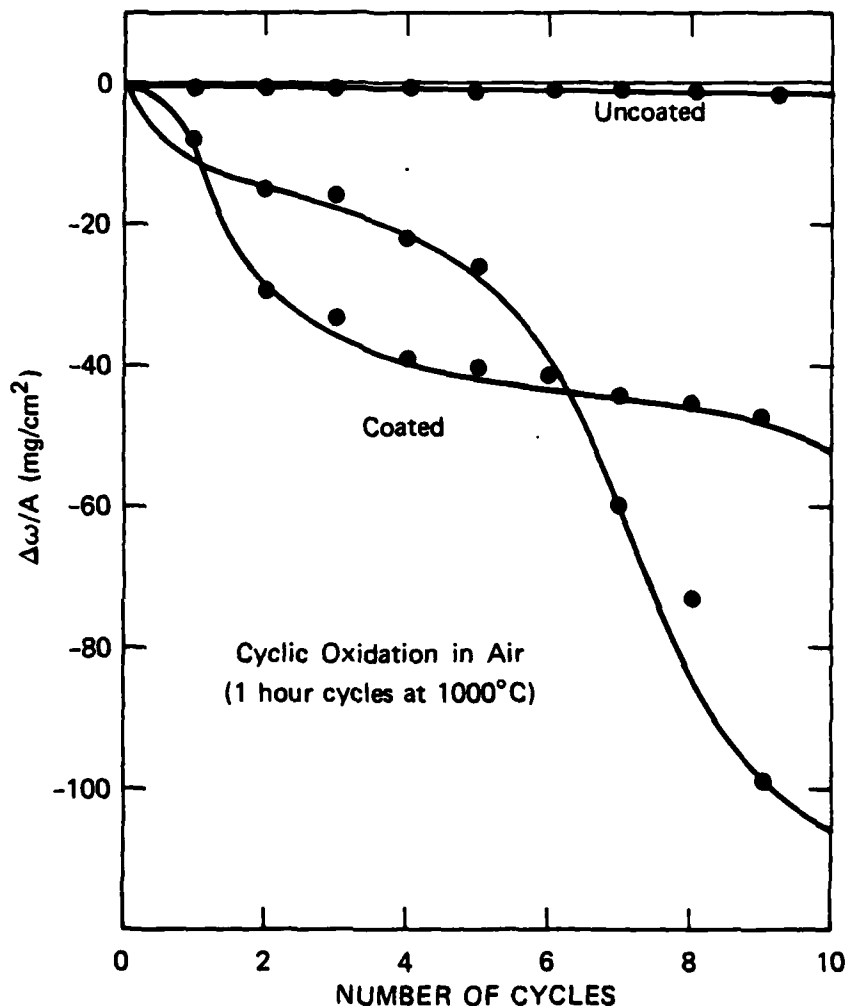
JA-2509-2

FIGURE 16 ISOTHERMAL WEIGHT GAIN VERSUS TIME PLOT FOR UNCOATED (CURVE 1) AND COATED (CURVE 2) MAR-M509; CURVE 3 AND 4 CORRESPOND TO SAMPLES THAT RECEIVED FINAL RECRYSTALLIZATION ANNEALING

The relatively close match of  $k_p$  for the oxidation of the coated alloy shown in curve 2 (Fig. 16) and those for the oxidation of nickel and cobalt suggests that the increase in the oxidation rate of the coated over the uncoated alloy is caused by the oxidation of nickel and cobalt at the external surface and within the coating layer. The formation of these fast growing oxides can eventually disrupt the  $\text{CeO}_2$  layer and can cause coating breakaway and spallation. This was confirmed by a moderate loss of coating adhesion, particularly near sample corner and edges during cooling from the oxidation temperature.

The isothermal weight gain data of the oxidation of coated MAR-M509 that received recrystallization annealing treatment is shown in curves 3 and 4 in Fig. 16. The oxidation rates, although slower than that of the nonrecrystallized sample (curve 2), are much faster than that of the uncoated alloy, which forms protective  $\text{Cr}_2\text{O}_3$  during exposure. Like the nonrecrystallized sample, the parabolic rate constants of the recrystallized samples are compatible with the oxidation of pure nickel and pure cobalt.

Preliminary evaluation of the spallation resistance of coated MAR-M509 was conducted by thermal cycling the samples at 1000°C (1 h hot, 20 min cold at room temperature). The cyclic oxidation results of coated and uncoated samples are shown in Fig 17. As expected, the fast oxidation of metallic nickel and cobalt above and within the coating leads to significant loss of adhesion and coating spallation. Spallation usually occurs at sample corners and edges where thermal stresses are perpendicular to the coating surface. The slight weight loss of the uncoated samples was due to the slow growth of  $\text{Cr}_2\text{O}_3$  layer, which readily spalls during cooling but regrows within the following exposure, again as a very thin layer.



JA-2509-3

FIGURE 17 RESULTS OF PRELIMINARY EVALUATION OF SPALLATION RESISTANCE OF COATED AND UNCOATED MAR-M509 UNDER THERMAL CYCLING CONDITIONS

#### IV GENERAL DISCUSSION

The present work has established the possibility of applying a duplex  $\text{CeO}_2$ -based coating on cobalt-base superalloys. The data presented so far show that the most promising coating was produced on the alloy MAR-M509. However, the results of preliminary evaluation of the coated alloys indicate that unacceptable oxidation rates result from the oxidation of metallic cobalt and nickel at the outer coating surface and within the coating layers. The volume ratio  $\gamma$  (volume of oxide/atomic volume of metal) of  $\text{NiO}$  and  $\text{CoO}$  are 1.65 and 1.86,<sup>18</sup> respectively. This will generate stresses within the oxide layer which can lead to breakaway and spallation.

It is important to emphasize that the final recrystallization treatment has not beneficially modified the coating microstructure or improved the coating quality as was originally expected. This treatment reduced the higher oxide  $\text{CeO}_2$ , which was useful as a thermal barrier, to the less stable sesquioxide  $\text{Ce}_2\text{O}_3$  which tends to oxidize even at low temperature. Consequently the final recrystallization annealing treatment must be eliminated and the processing conditions will be limited to three steps; hot-dipping, annealing, and internal oxidation.

Based on the above results, the following model for internal oxidation is proposed:

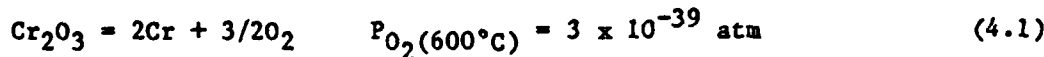
Initially, the major elements that are present at the unoxidized surface of hot-dipped and annealed samples are Ni, Co, Ce, Cr, and the intermetallic  $\text{CeCo}_2$  and  $\text{CeNi}_3$ . Cr exists only in very small concentrations as shown in Fig. 7. Upon initial exposure during the internal oxidation, chromium tends to form discrete  $\text{Cr}_2\text{O}_3$  particles rather than continuous scale. Cerium, which is abundant at the surface will be practically the only element to oxidize in-situ under the low  $P_{\text{O}_2}$  condition into  $\text{CeO}_2$  nuclei separated by nickel- and cobalt-rich areas. Once the  $\text{CeO}_2$  nuclei start to grow, the Ni/Co rich areas will expand laterally because the

cerium contained in them and in the intermetallics  $\text{CeCo}_2$  and  $\text{CeNi}_3$  will be removed.

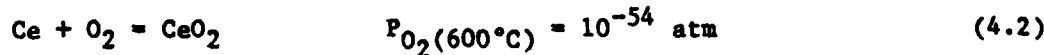
Further exposure will lead to the inward diffusion of oxygen across the nucleated  $\text{CeO}_2$  particles as well as through the unoxidized islands of nickel and cobalt at the surface. Oxygen will dissolve in the metal ahead of the interface where the cerium concentration is still high, leading to both inward and lateral growth of the  $\text{CeO}_2$ . The rate of  $\text{CeO}_2$  growth is probably fast enough for the unoxidized metals in this outer vicinity, mainly cobalt and nickel, to be incorporated by the growing oxide rather than to back-diffuse into the unoxidized alloy ahead of the interface.

Further growth of  $\text{CeO}_2$  will lead to the formation of a continuous external scale and isolate relatively large islands of Ni and Co at the original surface, while the inwardly growing  $\text{CeO}_2$  itself incorporates high proportions of both metals.

Once a continuous  $\text{CeO}_2$  layer has formed, the oxygen activity ahead of the interface drops below the dissociation pressures of  $\text{Cr}_2\text{O}_3$ :



Therefore chromium, mainly present in the large randomly distributed islands in the middle portion of the coating layer, will remain in the metallic form. However, the oxygen pressure remains higher than the value necessary to oxidize metallic cerium:



This pattern will continue during exposure across the rich cerium layer until the ingressing oxide/metal interface reaches the inner portion of the cerium-rich matrix that is relatively depleted in cerium.

Within the cerium depleted region, adjacent to the unaffected substrate, internal oxidation of cerium will predominate. The mechanism(s) of internal oxidation in this region will determine the morphology of the internal oxide particles and their distribution. Three different mechanisms are possible:

- (1) At equilibrium, the concentrations of the reacting species (cerium and dissolved oxygen) into the substrate immediately ahead of the interface are very high so that:

$$C^0\text{Ce} \times C^0\text{O}_2 \gg K_{sp}\text{CeO}_2 \quad (4.3)$$

where  $C^0\text{Ce}$  = concentration of metallic cerium

$C^0\text{O}_2$  = concentration of dissolved oxygen

$K_{sp}\text{CeO}_2$  = solubility product of  $\text{CeO}_2$  into the substrate.

Under this condition, spontaneous nucleation of discrete  $\text{CeO}_2$  spherical particles into the substrate matrix occurs. The driving force for the nucleation of these spherical particles is surface energy minimization.

- (2) The concentrations of the reacting species are very low so that:

$$C^0\text{Ce} \times C^0\text{O}_2 \ll K_{sp}\text{CeO}_2 \quad (4.4)$$

Thus no  $\text{CeO}_2$  particles will nucleate. Oxide growth in this case will proceed by an interfacial reaction between the outwardly diffusing cerium and oxygen diffusing inwardly across the scale.

- (3) The concentrations of the reacting species are moderate so that:

$$C^0\text{Ce} \times C^0\text{O}_2 > K_{sp}\text{CeO}_2 \quad (4.5)$$

Thus, limited spontaneous nucleation of  $\text{CeO}_2$  particles will occur and minimum surface energy will be attained by the growth of the already existing particles rather than the nucleation of new particles.

During internal oxidation, of the  $\text{CeO}_2$  depleted zone, condition (3) becomes operative and will lead to the deeper growth of  $\text{CeO}_2$  particles in the form of platelets or rod-like structures and will result in a fibrous oxide/metal configuration near the unaffected substrate (Fig. 10).

Finally, it is evident that the success of this coating as a thermal barrier largely depends on the elimination of metallic nickel and cobalt from the outer continuous  $\text{CeO}_2$  layer. We propose two approaches to achieve this purpose:

- (1) Introduce chromium and aluminum into the original coating melt ( $\text{Ce-Ni}$ ) to slow the oxidation rate. The presence of both elements in relatively small concentration (5-10 wt%)

will not lead to formation of continuous scale, but aluminum may oxidize internally, and cerium will oxidize as a continuous scale because of its high concentration. This will slow down the oxidation rate, which should allow the back diffusion of Ni and Co into the unoxidized alloy ahead of the interface.

- (2) After hot-dipping and annealing, the samples will be redipped into pure cerium metal to enrich the surface. Moderate annealing conditions (low annealing temperature for shorter duration) must be used to reduce the outward diffusion of cobalt from the substrate toward the coating surface.

## V FUTURE WORK

Based on this year's results we plan the following work for the next year's program:

1. Eliminate the incorporation of nickel and cobalt into the thermal barrier layer. Improved performance requires that the external ceramic layer should be exclusively of cerium dioxide ( $CeO_2$ ) that contains no metallic constituents. To achieve this goal, we will introduce chromium and aluminum into the original coating melt in concentrations lower than those required to form their oxides as external scales during subsequent internal oxidation. Alumina ( $Al_2O_3$ ) would be more stable than cerium oxide ( $CeO_2$ ) under the conditions of internal oxidation. If the volume fraction of aluminum in the cerium-rich surface zone is below the value necessary for transition to external oxidation, then internal alumina particles should form as a subscale ahead of the  $CeO_2$ /alloy interface. These particles should reduce the cross section through which inward diffusion of oxygen occurs (blocking effect). This is expected to slow down the growth rate of the continuous  $CeO_2$  scale, and thus allow enough time for the back diffusion of nickel and cobalt that are accumulated in the metal side of the interface, towards the substrate. The effect of this treatment on the oxidation resistance of the coated alloys will be investigated.
2. Study the mechanism of internal oxidation and determine the effects of temperature and oxygen pressure on the oxide microstructure.
3. Determine the resistance of dip-coated superalloys to hot corrosion by molten sulfates, primarily  $Na_2SO_4$  and  $Na_2SO_4/NaCl$  mixtures.
4. Evaluate the hot strength of dip-coated alloys using short-time tensile tests at high temperatures.
5. If time and funds permit, we plan to investigate the thermal properties of  $CeO_2$  layers.

## VI PUBLICATIONS, PRESENTATIONS AND PATENTS

- (1) I. M. Allam, "Dip Process Thermal Barrier Coating for Superalloys," paper presented at Bay Area High Temperature Corrosion meetings, organized by Professor D. P. Whittle at Lawrence Berkeley Laboratory, University of California, Berkeley, (December 1, 1981).
- (2) I. M. Allam and David J. Rowcliffe, "Dip Process Thermal Barrier Coatings for Superalloys," submitted to The International Conference on Metallurgical Coatings and Process Technology, to be held April 9, 1982, San Diego, California.
- (3) P. J. Jorgensen and R. W. Bartlett, "Process for Applying Thermal Barrier Coating to Metals and Resulting Products," U.S. Patent Application, 325,504 (November 27, 1981).
- (4) I. M. Allam and D. J. Rowcliffe, "Development of Zirconia Thermal Barrier Coating from Zr-Ni Eutectics," Invention Disclosure, SRI-Docket No. P-1752.

## REFERENCES

1. Engineering Property Data on Selected Ceramics, Vol. 3 - single oxide, Report No. MCIC-HB-07, published by Metals and Ceramics Information Center, (July 1981).
2. Engineer's Guide to High-Temperature Materials, ed. F. J. Clauss, published by Addison-Wesley series in Metallurgy and Materials Science (1969) p. 221.
3. Solid Electrolyte and Their Applications, ed. E. C. Subbarao, published by Plenum Press, N.Y. (1980) p. 270.
4. S. Stecura, "Two-layer Thermal Barrier Coatings for High Temperature Components," Cer. Bull. 56, No. 12 (1977) p. 1082.
5. R. G. Cooke and D. E. Lloyed, "Fabrication of Zirconia Bodies and Some Consideration of Their Thermal Shock Properties," published in Special Ceramics-5, Proceedings of the Fifth Symposium on Special Ceramics, ed. P. Popper, published by The British Ceramic Research Association, London (1971) p. 125.
6. J. W. Patten, R. W. Moss, M. A. Bayne, D. D. Hays, E. D. McClanahan and J. Fairbanks, "Development of Sputter Deposited Multilayered Ceramic/Metal Coating," Proceedings of the First Conference on Advanced Materials for Alternative-Fuel-Capable Directly Fired Heat Engines, ed. J. Fairbanks and J. Stringer (December 1979) p. 615.
7. D. S. Duvall, "Processing Technology for Advanced Metallic and Ceramic Turbine Airfoil Coatings," paper presented in the Second Conference on Advanced Materials for Alternative-Fuel-Capable Heat Engines held in Monterey, California (August 1981).
8. R. W. Bartlett and P. J. Jorgensen, "Microstructural Changes in SmCo<sub>5</sub> Caused by Oxygen, Sinter Annealing, and Thermal Aging," J. Less. Com. Metals, 37 (1974) p. 21
9. R. W. Bartlett and P. J. Jorgensen, "Microstructural Growth Kinetics of the Fibrous Composite Subscale Formed by Internal Oxidation of SmCo<sub>5</sub>," Met. Trans., 5 (1974) p. 355.
10. High-Temperature Materials and Technology, eds. I. E. Campbell and E. M. Sherwood, published by John Wiley & Sons, Inc., N.Y. (1967) p. 240.
11. High-Temperature Inorganic Coatings, ed. J. Huminik, Reinhold Publishing Corp., N.Y. (1963) p. 18.

12. O. Kubaschewski and C. B. Alcock, Metallurgical Thermochemistry, fifth edition, Pergamon Press, Oxford (1979).
13. Nonstoichiometry, Diffusion, and Electrical Conductivity in Binary Metal Oxides, ed. P. Kofstad, published by John Wiley & Sons, Inc., N.Y.(1971) p. 276.
14. G. Bayer, "Thermal Expansion Anisotropy of Oxide Compounds," published in Proceedings of the British Ceramic Society, Ceramics for Turbines and Other High Temperature Engineering Applications, Ed. D. J. Godfrey, published by the British Ceramic Society, Stoke-on-Trent, England (1973) p. 39.
15. I. M. Allam, R. W. Bartlett, and G. N. Krishnan, "Dip Process Thermal-barrier Coatings for Superalloys," SRI Final Report, AFOSR Contract No. F49620-79-C-0225 (June 1980).
16. M. Hansen, Constitution of Binary Alloys, second edition, McGraw-Hill Book Co., N.Y.(1950).
17. JANAF Thermochemical Tables, NSRDS-NBS37, U.S. Government Printing Office, Washington, DC (1971) and Supplement.
18. O. Kubaschewski and B. E. Hopkins, Oxidation of Metals and Alloys, second edition, published by Butterworths and Co., Ltd., London, England (1962).

